

# Numerical experiments on salt-finger convection

Jiro Yoshida\* and Hideki Nagashima

Department of Ocean Sciences, Tokyo University of Fisheries

---

\* Corresponding author. Fax +81-3-5463-0453

*E-mail address:* [jiroy@tokyo-u-fish.ac.jp](mailto:jiroy@tokyo-u-fish.ac.jp) (J. Yoshida)

## Abstract

Salt-finger convection is now widely recognized as an important mechanism for mixing heat and salt both vertically and laterally in the ocean. This article reviews numerical simulations of salt-finger. Salt-fingers were first produced in the laboratory in the mid-1960 when their structure and transport mechanisms were partially described. However, rapid diffusion of heat in the laboratory frustrates exact or conclusive understanding of many aspects of salt-fingers. Numerical simulation of salt-finger began in the 1980's. The rapid development of computational technology has brought great improvements in our understanding of salt-fingers. However, fully 3-D simulations that resolve all the scales present in salt-fingering, particularly in an oceanic environment where internal waves and turbulence are confounding influences, pose many more challenges for the future.

## Keywords

Density ratio, Flux ratio, Numerical experiments, Salt-finger, Prandtl Number, Stern Number

---

## Contents

1. <a href="#">Introduction</a> .....	2
2. <a href="#">Two-dimensional modeling of salt-finger convection</a> .....	3
3. <a href="#">Three-dimensional modeling of salt-finger convection</a> .....	14
4. <a href="#">Recommendation</a> .....	18
<a href="#">Acknowledgements</a> .....	22
<a href="#">References</a> .....	23

---

## 1. Introduction

Since the discovery of double-diffusive convection by Stommel, Arons & Blanchard (1956), "evidence has accumulated for the widespread presence of double-diffusion throughout the ocean" and for its "significant effects on global water-mass structure and the thermohaline convection" (Schmitt, 1998). The salt-fingering form of double-diffusion has particularly attracted interest because of its peculiar long thin cell structure and enhancement of the diapycnal transport of heat and salt, even when the net density gradient is stable. Furthermore, much of the upper kilometer of the ocean has conditions favorable for salt-fingering, namely warm salty water overlying cooler fresher water. Kluikov and Karlin (1995) suggested that two-thirds of world ocean is favorable for fingering convection. For example, in the tropics, surface evaporation exceeds precipitation and heating exceeds cooling, producing these conditions. In contrast, the diffusive convection form of double-diffusion is commonly found in polar water where cool fresh water overlies warmer saltier water.

Salt-fingering has been investigated both theoretically and experimentally. Theoretical analysis of salt-fingers was first considered by Stern (1960). Its subsequent developments are summarized by Kunze (2003) in this issue. Salt-fingering laboratory experiments were first conducted by Turner and Stommel (1964). Subsequent works are summarized by Schmitt (2003) in this issue. Analytical and modeling efforts have focused on the onset and stability of salt-fingers, their diapycnal heat and salt transports, layer formation, and interaction with internal waves and shear-driven turbulence. Governing parameters, vertical and horizontal scales for fingers, a laboratory  $4/3$  power law for heat and salt fluxes, a flux ratio, and stability

criteria (e.g., Stern number (Stern, 1969; Holyer, 1981)) have resulted from this research.

These results were at first difficult to apply to the ocean because sensors were too crude to detect salt-finger microstructure. With the introduction of precise CTD, shadowgraph and microstructure sensors on towed bodies and profilers, improved information about vertical and horizontal ocean microstructure has accumulated. These measurements have revealed both agreement and contradictions with respect to the expected finger structure, heat and salt fluxes, and fingering layer thickness. Many of the discrepancies may be due to the fact that a majority of experiments have been conducted using sugar and salt, with sugar diffusing slower than salt. The sugar-salt system has a Prandtl number of 1000 compared to the oceanic molecular Prandtl number of 7. An additional problem has been conducting laboratory experiments over a wide parameter range.

The direct numerical simulation of salt-fingers can overcome some of these limitations. Piacsek and Toomre (1980) first successfully produced 2-D salt-fingers numerically. Their computational domain was crude by modern standards. With the development of high-performance computers, the details of fingers and the resulting turbulent motion are now much better resolved. These outputs are now available to improve our knowledge directly. In the following sections, we will review these efforts and discuss future numerical simulations that are needed.

## **2. Two-dimensional modeling of salt-finger convection**

Following Piacsek and Toomre (1980), Piacsek, Brummell & McDonald (1988), Shen (1989), Whitfield, Holloway & Holyer (1989), Shen and Veronis (1991), Shen

(1993), Shen (1995), Shen and Veronis (1997), Stern and Radko (1998), Özgökmen, Esenkov & Olson (1998), Özgökmen and Esenkov (1998) and Merryfield and Grinder (unpublished) have all conducted numerical simulations of two-dimensional salt-fingers using the same vorticity, heat and salt equations. Following Shen and Veronis, we take  $x$  as horizontal and  $z$  as vertically upward. The non-dimensional equations are:

Vorticity Equation

$$\frac{\partial}{\partial t} \nabla^2 \Psi - J(\Psi, \nabla^2 \Psi) = -\sigma R_T \frac{\partial T}{\partial x} + \sigma R_S \frac{\partial S}{\partial x} + \sigma \nabla^4 \Psi$$

Heat Equation

$$\frac{\partial T}{\partial t} - J(\Psi, T) = \nabla^2 T$$

Salt Equation

$$\frac{\partial S}{\partial t} - J(\Psi, S) = \tau \nabla^2 S,$$

where  $\Psi$  is the stream function defined in terms of horizontal and vertical velocity

$$u = \frac{\partial \Psi}{\partial z}, \quad v = -\frac{\partial \Psi}{\partial x} \quad \text{and} \quad J \text{ is the Jacobian defined as } J(a, b) = \frac{\partial a}{\partial x} \cdot \frac{\partial b}{\partial z} - \frac{\partial a}{\partial z} \cdot \frac{\partial b}{\partial x}.$$

The governing non-dimensional parameters are the Prandtl number  $\sigma = \frac{\nu}{\kappa_T}$ , the

Lewis number  $\tau = \frac{\kappa_S}{\kappa_T}$ , the thermal Rayleigh number  $R_T = \frac{g \alpha \Delta T d^3}{\kappa_T \nu}$  and the

saline Rayleigh number  $R_S = \frac{g \beta \Delta S d^3}{\kappa_T \nu}$ . The definitions and other important

parameters for the salt-finger problem are listed in [Table 1](#)

In this table,  $\nu, \kappa_T$  and  $\kappa_S$  are the molecular diffusivities of momentum, heat and salt;  $g$  the acceleration due to gravity;  $\alpha$  and  $\beta$  thermal expansion and saline contraction coefficients;  $\Delta T$  and  $\Delta S$  the temperature and salinity difference across the computational domain. When the calculation is initiated with a sharp fingering-favorable interface separating homogeneous layers (Piacsek and Toomre,

1980; Shen, 1989; 1993),  $\Delta T$  and  $\Delta S$  can be defined as the property differences between these homogeneous layers. When background temperature and salinity fields are continuously (linearly) stratified (Whitfield et al., 1989; Shen, 1994; Shen and Veronis, 1997; Stern and Radko, 1998; Özgökmen et al. 1998; Merryfield and Grinder, unpublished), they are defined as the difference between the top and bottom values. Using these property contrasts, one can define a density ratio  $R\rho = \alpha \Delta T / \beta \Delta S$ , which characterizes salt-finger behavior. For  $1 < R\rho < 2$ , salt-finger growth rates are large and salt-fingers are thought to actively transport heat and salt in the ocean. The thermal and saline Rayleigh numbers are related by  $R_T = R\rho \cdot R_S$ . We can also define the flux ratio of the heat- and salt-flux contributions to the buoyancy-flux  $\gamma = \alpha F_T / \beta F_S = f(R\rho)$  where  $F_S$  and  $F_T$  are the diapycnal salt and heat fluxes. The length scale  $d$  was taken as the height of the fluid layer in the stability analysis of Baines and Gill (1969). However, Shen and Veronis (1997), Stern and Radko (1998) and Merryfield and Grinder (unpublished) used the width of the fastest growing finger ( $d = (\kappa_T \nu / g \bar{T}_z)^{1/4}$ ) as the characteristic length scale because faster diffusion of heat than salt is essential to salt-fingers. With the introduction of such a length-scale, the characteristic timescale is defined as  $d^2 / \kappa_T$ , and the velocity scale as  $\kappa_T / d$ . Özgökmen et al. (1998) used the width of the computational domain as the length-scale and viscosity instead of heat diffusivity. They introduced the Schmidt number  $Sc = \frac{\nu}{\kappa_S}$  in the salt equation. Another important parameter in [Table 1](#) is the Stern number. The Stern number is a criterion that governs the stability of fingers interacting with a large-scale internal wave field (Stern, 1969). When the net vertical buoyancy flux which feeds the internal waves exceeds the viscous dissipation, salt-fingers were argued to become unstable. The critical value was defined as 1/3 for steady fingers by Holyer (1981). Kunze (1987) used a finger Richardson number

constraint that proved equivalent to the Stern number. These stability analyses were applied to explain finger fluxes, flux ratios and interface thicknesses in the real ocean (Hebert, 1988; Schmitt 1988).

Numerical simulations have been conducted by using various combinations of the non-dimensional parameters (Table 1) to produce fingering, and examine theoretically derived salt-finger flux laws and stability criteria. The parameters used in the experiments cited above are summarized in Table 2. In the following chapters, we will briefly describe the results of each calculation.

1) Piacsek and Toomre (1980):

Piacsek and Toomre (1980) did not non-dimensionalize their equations. They used  $\sigma = 6.8$ ,  $\tau = 0.01$  (heat-salt system),  $R\rho = 3, 5$  and  $7$ . Their domain was  $1.25$  cm or  $2.5$  cm wide and  $2.50$  cm or  $5.00$  cm high. Grid spacing was  $0.02$  cm in both the vertical and horizontal so that their grids with  $64 \times 128$  or  $128 \times 256$ . Their simulations were initialized with two homogeneous layers separated by a sharp fingering-favorable interface. Heat- and salt-fluxes were imposed at the upper and lower boundaries while lateral boundaries were periodic. Their simulations resolved  $8$  fingers (Figure 1) and clearly reproduced the blobs at the tips of the fingers seen in laboratory heat-salt experiments. Faster diffusion of heat results in a smooth linear profile while slower diffusion of salt creates a homogeneous salinity profile in the finger region. These simulations did not reach an equilibrium state. They exhibited a linear dependence of the flux ratio  $\gamma$  on the density ratio  $R\rho$ , not in agreement with laboratory experiments. The authors attributed this discrepancy to the absence of convecting layers above and below fingering layer, which may play an important role in the stability of fingers. In the following paper (Piacsek et al., 1988), they attempted

to build multi-layers and considered both salt-fingering and diffusive-layering situations, and showed that the layers didn't get beyond 3 layers.

2) Whitfield et al. (1989):

In the experiments of Whitfield et al. (1989), the Prandtl number  $3 \leq \sigma \leq 10$  and the Lewis number  $0.1 < \tau \leq 0.5$ , so they simulated neither heat-salt nor sugar-salt-fingers. The inverse buoyancy frequency  $N^{-1}$  was used as a time scale and  $(\kappa_T / N)^{1/2}$  as a length scale, so the Rayleigh numbers shown in Table.1 did not explicitly appear in their analysis. They investigated 5 cases spanning  $1.1 < R\rho < 2.5$ , using a fingering-favorable background density structure with uniform stratification of faster (T) and slower (S) diffusing components. Steplike T and S perturbations were imposed as initial conditions. Boundary conditions were periodic in both horizontal and vertical. Grids were  $128 \times 256$  and  $256 \times 256$ . In the coarse grid case, 6 fingers were resolved (Figure 2). These simulations reproduced blob structures. But the flux ratio did not agree with either theoretical (Kunze, 1987) or laboratory (Schmitt, 1979a; Griffiths and Ruddick, 1980; McDougall and Taylor, 1984) predictions. The authors attributed this discrepancy to the mechanisms that govern salt-finger stability. The Stern number of their simulations was large so that collective instability, or equivalently shear instability, did not appear to apply to their fingers. They concluded that this might be an artifact of the computation.

3) Shen (1989;1993;1995), Shen and Veronis (1990;1997)

Shen has made a tremendous contribution to understanding salt-finger dynamics through numerical simulations. Hereafter, we shall abbreviate his papers as Shen89,

Shen90, Shen93, Shen95 and Shen97. .

As was the case in Whitfield et al. (1989), the Prandtl and the Lewis numbers in Shen 89  $\sigma = 1, \tau = 0.01$ ,  $\sigma = 1, \tau = 0.5$  and  $\sigma = 2, \tau = 0.5$  were set to resolve viscous and diffusive time- and length-scales fully, so did not correspond to a realistic fluid. The density ratio was set to 2 in all simulations. Density Rayleigh number was used and set to 22.3, 25.0 and 8.8. 2-D simulations were carried out on  $256 \times 258$  grids with periodic boundary conditions in the vertical and horizontal. The simulations were initialized with a small white-noise perturbation applied to the sharp interface separating two homogeneous layers.

The evolution of temperature and salinity fields is shown in [Figure 3](#). Many fingers are present and the blob structures evident in previous simulations are seen in the salinity field here as well. However, subsequent development differs from past simulations. After the onset of mushroom plumes, narrow fingers and convective plumes co-exist with the fingering interface remaining at mid-depth. This is consistent with the previous laboratory experiments.

The evolution of density, temperature and salinity profiles are shown in [Figure 4](#). The fingering interface is identifiable as the layer of steep gradients. Due to the differing molecular diffusivities of heat and salt, the salinity profiles have a rather weak gradient with more small-scale structure than temperature profiles. Shen89 attributes these differences to the fact that convecting fluxes due to fingers dominate the salinity interface while molecular diffusion dominates the temperature interface. The most interesting aspect of this simulation is the transition to turbulent convection at the edge of the fingering interface while the interface continues to thicken. This is caused by frequent density inversions at the edge of the interface. The Stern number

exceeds  $1/3$  (Holyer, 1981) in all three cases. Shen89 concluded that the Rayleigh-Taylor type instability occurred at the edge of the fingers.

In Shen 93, the numerical simulations were extended to the oceanic range of  $\sigma = 7, \tau = 0.01$  and  $R\rho$  spanned 1.2 to 4.0. The thermal Rayleigh number was chosen to resolve 24 fingers in the numerical domain of  $512 \times 512$  grid points. Initial stratification was as in Shen89 and again boundary conditions were periodic in the vertical and horizontal. These simulations investigated the laboratory and analytical flux laws. The flux ratio, the proportionality constant  $C$  of the  $4/3$  flux law, and the Stern number from these simulations and previous laboratory experiments are shown as a function of density ratio in [Figure 5](#). Functional dependences were not derived but numerical and laboratory values agree fairly well. The flux ratio agrees with Schmitt's (1979b) fastest-growing finger model, but not Howard and Veronis's (1987) steady maximum buoyancy-flux prediction. On the other hand, the square wave-like structure of the horizontal salt field agrees with Howard and Veronis (1987) rather than Schmitt (1979b). In Schmitt's model, the mean vertical salt gradient exists because of salt diffusion across finger cells and a sinusoidal wave form is assumed while, in Howard and Veronis (1987), lateral diffusion of salt is negligible and a square wave form is assumed for analytic simplicity. To show that the maximum vertical flux hypothesis is not appropriate, Shen93 proposed a model in which the mode that maximizes the amplitude of the vertical finger velocity is preferred. The calculated Stern numbers show the same trend as in laboratory experiments but are slightly smaller.

Shen95 investigated the role of temperature and salinity stratification in more detail, considering a thick stratified layer with uniform temperature and salinity gradients

and including vertical diffusion of heat and salt by these gradients. The Rayleigh number based on the vertical scale is large. Density ratios of 2-8 were considered. Other parameter ranges and domain configurations were as in Shen93. The resulting growth of fingers and salt-fluxes is limited by instability of finger cells. An equilibrium state was achieved in which the energy dissipation was balanced by the buoyancy forcing. Equilibrium fluxes were proportional to the mean background gradients, in contrast to Shen93 where fluxes depended on the inverse 1/2 power on salinity gradients of finite extent.

Shen97 summarized previous work on oceanic 2-layer heat-salt systems. They produced salt-fingers for various thermal and saline Rayleigh numbers for density ratios of 1.5-3 in a  $512 \times 1024$  numerical domain. Other conditions were as in Shen89. Their flux ratios were high for saline Rayleigh numbers  $R_s = 1.83 \times 10^6$  and  $R_\rho = 1.5$ , in agreement with laboratory experiments by Turner (1967) and Schmitt (1979a). When the Rayleigh numbers were low, they found spatial period-doubling (Figure 6). The fingertip blob structures observed in previous numerical and laboratory experiments were also found in these simulations which resolved 8 finger pairs. At the intruding tip of each finger, an umbrella-shaped structure formed and spread laterally. However, interactions between these blobs inhibited lateral spreading. Wavy motion then appeared that accelerated sandwiched blobs, thinning their necks until a new blob formed in the upper or lower layer. This spatial period-doubling is analogous to the upscale energy cascade observed in 2-D turbulence. Period-doubling occurred three times in their simulation domain. Large-scale eddies formed in the upper and lower layers.

4) Özgökmen et al. (1998):

In this simulation, the Prandtl and Lewis numbers were chosen to be  $\sigma = 100$ ,  $\tau = 1/30$ , equivalent to a starch-sugar system in order to adequately resolve the salt-fingers in a  $301 \times 113$  computational domain. They used a density ratio  $R\rho = 1.6$  and thermal Rayleigh number  $R_T = 6 \times 10^7$  with initially uniform vertical gradients. The top and bottom boundary conditions differed from previous simulations in being free-slip and zero mass-, heat- and salt-flux, equivalent to a closed box or laboratory tank. Initially, sinusoidal perturbations are imposed with wavelengths larger than steady fingers based on the initial thermal Rayleigh number in order to speed up the numerical calculation. The evolution of the stream function, temperature and salinity fields are shown in [Figure 7](#) as well as horizontally-averaged vertical profiles of temperature, salinity and density.

At first, large-scale fingers grew at mid-depth. The top and bottom boundary conditions homogenize temperature and salinity near the upper and lower boundaries ([Figure 7a](#)). As time progresses, smaller scale fingers tipped by blobs appear with a width scale consistent with the steady finger model. The vertical domain of the fingers thins as large-scale convective motions near the top and bottom homogenize the fluid, forming an equilibrium of well-mixed layers sandwiching a high-gradient fingering interface. Throughout, the temperature profile is smoother than the salinity profile. Both salinity and density inversions are evident as the upper and lower layers mix ([Figure 7b](#)). At the latter stage, pairing of finger blobs (period doubling) occurs and detached fingers form umbrella-like plumes. The density gradient in the fingering interface increases, indicating that the buoyancy-flux is countergradient as also observed by Shen89, Shen95 and Shen97.

The equilibrium state is also confirmed by the time evolution of the temperature difference between the upper and lower layers. While the salinity difference decreases continuously due to the efficient finger transport of salt, temperature differences weaken only through vertical molecular diffusion.

Focusing on the instability of fingers and subsequent blob formation, Özgökmen et al. (1998) calculated the Stern number. Initially, the Stern number increases rapidly until it attains its maximum value when the homogeneous convective layers form near the upper and lower boundaries. It then gradually decreases below the 'critical value' of  $1/3$  during equilibrium. While this behavior seems to be explicable by the collective instability mechanism, the numerical results show that blob formation and detachment exist even when the Stern number exceeds the critical value. The authors concluded that the instability mechanism for controlling finger fluxes remains unknown. The vertical flux ratio and  $4/3$  power law were also examined. The flux ratio achieves an equilibrium value of about 0.55, consistent with the predictions of Schmitt (1983). A  $4/3$  power law is consistent except during the initial and final stages of the simulation when equilibrium is not maintained.

Özgökmen and Esenkov (1998) examined the effect of nonlinearity in the equation of state by adding quadratic dependence of density on temperature. They showed that the stabilizing effect of temperature is enhanced, and as a result, the growth of salt-fingers is delayed. Once the salt-fingers are established, the nonlinear effect increases the buoyancy effect acting on the downward-going fingers more than it decreases that acting on upward-going ones. This effect results in narrower and faster growing downward fingers than upward ones.

5) Merryfield and Grindler (unpublished)

In this simulation, the oceanic heat-salt system ( $\sigma=7, \tau=0.01$ ) is examined with density ratio  $R\rho$  ranging from 1.25 to 20 so as to compare the diffusivities of heat and salt with oceanic observations. Background temperature and salinity gradients are uniform, and doubly-periodic boundary conditions are applied. Grid sizes are varied from  $256 \times 256$  to  $512 \times 512$  for the temperature field and from  $512 \times 512$  to  $1024 \times 1024$  for the salinity field according so as to fully resolve the salinity field. In their calculation, vertically elongated salt-fingers are developed, and broken up into blobs by a *secondary instability* (not by collective instability), as seen in the previous numerical experiment cited above. They also showed that fingering structure is disordered at low  $R\rho$ , which agrees with laboratory observed fingers (e.g. Shirtcliffe and Turner, 1970, see [Figure 8](#)). Spatially and temporally averaged effective heat and salt diffusivities are compared with those obtained at the NATRE site (St. Laurent and Schmitt, 1999) and in the C-SALT area (Fleury and Lueck, 1991) in [Figure 9](#). Numerically obtained diffusivities are in good agreement with those obtained at NATRE, but larger than those at C-SALT. This tendency is also shown in the horizontal temperature gradient spectra ([Figure 10](#)). The shapes of the spectra resemble each other, but the power levels of the numerical spectra are larger than the observed one at all wave numbers. These discrepancies are attributed to the fact that presence of shear should affect the strength of salt-fingering at the C-SALT site irrespective of the low-density ratio. Merryfield and Grindler (unpublished) also compared the density flux ratio  $\gamma$  with the fastest growing finger model of Schmitt (1979b) ([Figure 11](#)). The tendencies show fairly good agreement, but the functional dependence on  $R\rho$  is not given explicitly. The Stern number criterion is also examined. It shows that as  $R\rho$  is decreased towards unity, the Stern number

becomes large, as does the finger Reynolds number. This corresponds to an enhanced tendency of fingers to break up into blobs at low  $R\rho$  (see [Figure 8](#)). The temperature variance spectrum for  $R\rho=2$  shows fairly good agreement with that reported by Gargett and Schmitt (1982).

### **3. Three-dimensional modeling of salt-finger convection**

The obstacles to reproducing salt-finger convection in three dimensions are considerable. Resolving salt-finger structure in 3-D is difficult and there are few laboratory visualizations with which to compare the results. The few laboratory observations of the plan-form structure reveal regular rectangular cell structures that resemble classical Rayleigh-Benard cells (Shirtcliffe and Turner, 1970) or else sheets in the presence of uniform vertical shear (Linden, 1974). Osborn (1991) observed asymmetric salt fountains in the ocean, revealing the potential relevance of three-dimensional structure. Using 3-D linear theory, Schmitt (1994) found a rich variety of salt-finger plan-forms with the same growth rate, including an asymmetric finger similar to Osborn's observation.

Motivated by this result, Nagashima et al. (1997) performed 3-D numerical simulations of salt-fingers in the heat and salt system, using recently developed software called  $\alpha$ -FLOW in which a linearized equation of state is used in conjunction with the momentum, heat and salt equations. A numerical domain of 1.25cm by 1.25cm by 5cm high is used. All boundaries are slippery and allow no fluxes. The box is  $64 \times 64 \times 64$  grid points with grid sizes of 0.2 and 0.8 mm in the horizontal and vertical, respectively. The upper (lower) half of the box is occupied by warm and salty (cool and fresh) water. Initially, random disturbances are imposed just below the interface. Numerical simulations were carried out for three cases. Case 1

has the same initial temperature and salinity differences as Piacsek and Toomre (1980), and in cases 2 and 3 salinity differences are set to be 8 and 16 times larger than that of Case 1 to illustrate the dependence of finger scale and salt-flux on salinity difference. Small-scale undulations are found in and near the interface. After a while, salt-fingers of preferred horizontal scale develop as shown in [Figure 12](#). Mushroom structures form at the tips of the fingers and are seen in the horizontal plane corresponding to the initial position of the interface ([Figure 13, left](#)), irregular salt-fingers are apparent in salt concentration, consistent with a rich variety of finger forms (Schmitt, 1994). In Case 1, the preferred horizontal scale estimated by 2-D Fourier analysis is 3.72 mm, or 0.3 of the domain width, consistent with the 2-D model of Piacsek and Toomre (1980). In Case 3 ([Figure 13, right](#)), horizontal scales are smaller than in Case 1, only 1.86 mm. The scale of the fingers depends on the initial temperature difference as  $\Delta T^{1/4}$ , consistent with theory (Stern, 1960; Schmitt, 1981). The maximum salt-flux depends on salinity difference  $\Delta S^{4/3}$ . The Stern number was not estimated in this study. Structures resembled those in 2-D simulations, with blobs (mushrooms) formed at the finger tips. However, these blobs did not break up or detach as in Shen89, Shen97, Özgökmen et al. (1998) and Merryfield and Grindler (unpublished). No well-defined large-scale structures were observed even though the flux measurements indicate development of an equilibrium state. Shen97 suggest that period-doubling would not occur in three dimensions, and that overturning convection would be more localized. Period-doubling and large-scale eddies were not observed by Nagashima et al. (1997). These features need more investigation.

Recently, Stern and Radko (1998), Radko and Stern (1999) and Radko and Stern (2000) tried to simulate salt-finger convection in two- and three-dimensions. A high

Prandtl number ( $\sigma \approx 10^3$ ) sugar and salt system is considered; they neglect the nonlinear terms in the momentum equation, but not in the temperature and salinity equations. They also investigate the behavior of salt-fingers at the marginally stable limit when the density ratio  $R\rho$  is nearly equal to the Lewis number  $\tau$ . In this context, they introduced a new parameter defined as  $\varepsilon = (R\rho\tau)^{-1} - 1$ . In their calculation, background temperature and salinity gradients are uniform and remain unchanged with time, and temperature perturbation is initialized using rolls or square cells for horizontal planform:

$$T' = 0.2 \sin(mz) \cos(kx + ly) \quad \text{for roll and}$$

$$T' = 0.2 \sin(mz) \cos(kx) \cos(ly) \quad \text{for square cell,}$$

where  $k = l = k_0 / \sqrt{2}$ ,  $m/k_0 = \mu$ .  $\mu$  is the aspect ratio defined as the ratio of the horizontal wave-length of the fastest growing finger to the maximum vertical wave-length superposed on the domain.

In the case where the computational domain is not bounded (periodic boundary condition in three dimensions), Radko and Stern (1999) reproduce salt-fingers with various aspect ratios. They showed that the initial two-dimensional finger is replaced by three-dimensional fingers having planforms consisting of three-dimensional square cells and two-dimensional rolls (Figure 14). This three-dimensional finger reaches a statistically steady state having larger heat flux than a two-dimensional finger with same aspect ratio (Stern and Radko, 1998). Vertical structure shows the dominance of up and down going finger structure (vertical wave-number is 0, they called this mode the elevator mode), and the existence of three dimensional round eddies having vertical scales comparable with the basic finger width scale (Figure 15). They proposed a mechanism for equilibrating the elevator (salt-fingering) mode in

three-dimensions by a triad energy transfer between round eddies (basic and sub-harmonics) and the elevator mode. Namely, small-scale waves seen in [Figure 15](#) transfer heat and salt laterally between up and down going (elevator mode) fingers, and equilibrate the growth of fingers. Extended to small values of the density ratio, their calculations showed the systematic increase of heat flux with decreasing density ratio, and a flux ratio in quite good agreement with that obtained by Griffiths and Ruddick (1980) for density ratios ranging from 2.6 to 1.8.

An additional experiment was done with the calculation domain bounded by horizontal rigid and slippery surface with constant temperature and salinity, in order to compare with the laboratory run-down experiments (e.g. Griffiths and Ruddick, 1980). Motion was initiated as two-dimensional rolls, and showed the transition from two-dimensional rolls to three-dimensional square cells in steady state. The planform shows very regular square cell structure and a vertically coherent elevator mode with thin boundary layers on top and bottom. Density flux ratio again showed fairly good agreement with Griffiths and Ruddick (1980).

The behavior of three-dimensional fingers and the role of the boundary layers are investigated in more detail by Radko and Stern (2000). Horizontal distributions of the temperature field at mid-depth ([Figure 16a](#)) and near the boundary ([Figure 16b](#)) show that the square cell structure is distinct near the boundary, with mixed roll and square cell structure at mid-depth. Vertical temperature structure ([Figure 16c](#)) shows the existence of boundary layers near top and bottom. Those layers were not seen in the unbounded model. The transition (three-dimensional instability of the boundary layer) from two-dimensional rolls to three-dimensional square cells first occurred near the boundary, then proceeded to mid-depth ([Figure 17](#)). This tendency is enhanced when

the density ratio is sufficiently small ( $R\rho < 2$ ) and the local thermohaline Rayleigh number based on the thickness of boundary layer exceeds the range of 1000-2000 (Figure 18). Three dimensional structure generated near the boundary penetrates much more of inner region much more in the case of high Rayleigh number (Fig. 18b). The proportionality constant  $C$  of the 4/3 flux law as determined by the numerical calculations is compared with asymptotic ( $\varepsilon \rightarrow 0$ , which means  $R\rho \rightarrow 1/\tau$ ) analysis in Fig. 19a. Fig. 19b shows a similar comparison for the experimental data of Taylor and Veronis (1996). Except at smaller values of  $R\rho$  ( $\varepsilon$  becomes  $O(1)$ , and the asymptotic approximation fails at this limit), the agreement among asymptotic curve, numerical results and laboratory results seems satisfactory.

#### 4. Recommendations

As reviewed briefly here, two-dimensional simulations of salt-fingers showed fairly good agreement with laboratory results for flux laws, 4/3 power law, horizontal scale and structure. However, the stability of salt-fingers is itself not yet fully understood. Since Stern (1969) proposed a collective instability theory, salt-finger instability has been investigated in various contexts (Holyer, 1981; Veronis, 1987; Howard and Veronis, 1987). The Stern number criterion seems to be sufficient to determine instability of fingers, with possible additional minor dependence on density ratio, Prandtl number and Lewis number (Shen, 1993). However, these studies suggest that collective instability is not the sole mechanism of salt-finger instability, but only one of a myriad of possible instability modes. In fact, Shen's series of experiments and those of Özgökmen et al. (1998) revealed that both interactions among the blobs that form at finger tips and disorganized motions are important for secondary instability of fingers, and the formation of large scale convective motions. However, the large scale

convective motion that forms in the homogeneous mixing layers may be induced by different processes in these experiments since boundary conditions are periodic in Shen (1995), Shen (1997) and Merryfield and Grinder (unpublished) but insulated and slippery in Özgökmen et al. (1998). Moon (1998) investigated numerically the mechanism of the generation of a large convective cell through interactions among vortex pairs in an ideal situation in which the viscosity and density variation are neglected. He showed that large scale convection results from the collision of finger tips and should be accompanied by a small scale vortex pair moving in the opposite direction. Recent three-dimensional simulations by Radko and Stern (1999, 2000) revealed the importance of the boundary layer instability near the rigid surface in the sugar/salt system, and elucidate the transition from two-dimensional rolls to square cells.

As to the finger instability itself, the growth of instability to finite amplitude can bring about equilibration of finger fluxes when the thickness of the fingering zone or interface is much greater than the finger cell width (Shen, 1995; Stern and Radko, 1998; Merryfield and Grinder, unpublished). This instability of fingers results in transition of finger structure from laminar to turbulent at low density ratio as is often seen in the laboratory. Since salt-finger theories have traditionally assumed coherent laminar finger structure, this transition suggests that new theories for turbulent salt-finger should be developed, and examined by the numerical results cited above.

In the oceanic context, Schmitt (1988) found that the Stern number criterion still has importance. He showed that calculated buoyancy flux and salt eddy diffusivity from C-SALT data based on Stern number criterion well agreed with those from dissipation rates by direct microstructure measurements. Hebert (1988) used Kunze's

(1987) thick and thin interface models with a Richardson number criterion equivalent to the Stern number to show that the thick interface model in which salt-fingers do not extend across the entire vertical extent of the fingering-favorable layer gave reasonable estimates of finger fluxes in a Meddy. However, the laboratory  $4/3$  flux law overestimates fluxes inferred from bulk budgets in both cases. As was noted in the beginning of this section, laboratory flux laws and  $4/3$  power law are well reproduced by the numerical results, but these discrepancies suggest that there may be fundamental differences between the experimental setups and the real ocean, including stratification, background turbulence, vertical shear, etc. In fact, the thermal Rayleigh numbers used in numerical experiments ranged from  $O(10^2)$  to  $O(10^7)$ , while the oceanic value determined from C-SALT data (Gregg, 1988) is  $O(10^{13})$ . This point should be examined in future numerical experiment. Thus our first recommendation is: To conduct two- or three-dimensional numerical simulations focusing upon the interaction among salt-finger and turbulence, velocity shear and internal wave field.

As pointed out above, blobs and their interactions are essential to finger structure, but might be different in two-dimensional and three-dimensional simulations, so that the resulting finger instability might be different in these two cases. In Schmitt's (1994) linear model of triangular and asymmetric fingers, he suggests that a rich variety of planforms may be possible with the same growth rate. Radko and Stern (1999, 2000) gave an interesting insight to these mechanisms, however, their experiments were conducted in the sugar/salt system, and the non-linear terms in the momentum equation was neglected. In other three-dimensional experiments by Nagashima et al. (1997), focus was on the early development of fingers in heat/salt

system, and not their end state.

Therefore, our second recommendation is

- To conduct three-dimensional numerical modeling of salt-fingers under suitable conditions (Prandtl, Lewis and Rayleigh numbers having oceanic values), and to investigate the transition mechanism from two-dimensional to three-dimensional structure.

## **Acknowledgements**

The authors express their sincere thanks to Yuli Chashechkin and Joe Fernando who co-chaired our SCOR working group (WG 108). Thanks are extended to Drs. Eric Kunze, Ann Gargett and Hiroshi Niino for their valuable comments. Their efforts greatly improved this manuscript. We also express our thanks to Drs. Özgökmen, Merryfield and Radko for sending us preprints and draft manuscripts. Two anonymous reviewers are greatly acknowledged. Their comments especially improved section 4.

## References

- Baines, P.G., & Gill, A.E. (1969). On thermohaline convection with linear gradients. *Journal of Fluid Mechanics*, 37(2), 289-306.
- Fleury, M., & Lueck, R.G. (1991). Fluxes across a thermohaline interface. *Deep-Sea Research*, 38(7), 745-769.
- Gargett, A. E., & Schmitt, R.W. (1982). Observations of salt fingers in the central waters of the eastern North Pacific. *Journal of Geophysical Research*, 87(C10), 8017-8029.
- Gregg, M.C., (1988). Mixing in the thermohaline staircase east of Barbados. In *Small Scale Turbulence and Mixing in the Ocean*, eds. J.C.J. Nihoul and B.M. Jamart, Elsevier Oceanography Ser., 46, 453-470.
- Griffiths, R.W., & Ruddick, B.R. (1980). Accurate fluxes across a salt-sugar finger interface deduced from direct density measurements. *Journal of Fluid Mechanics*, 99(1), 5-95.
- Hebert, D. (1988). Estimates of salt-finger fluxes. *Deep-Sea Res.*, 35(12), 1887-1901.
- Holyer, J.Y. (1981). On the collective instability of salt fingers. *Journal of Fluid Mechanics.*, 110, 195-208.
- Howard, L.N., & Veronis, G. (1987). The salt-finger zone, *Journal of Fluid Mechanics*, 183, 1-23.
- Kluikov, Ye. Yu., & Karlin, L.N. (1995). A model of the ocean thermocline stepwise stratification caused by double diffusion. In *Double-Diffusive Convection*, A. Brandt and J. Fernando, Eds., AGU Geophysical Monograph 94, 287-292.
- Kunze, E., (1987). Limits on growing, finite-length salt fingers: A Richardson number constraint. *Journal of Marine Research.*, 45, 533-556.
- Kunze, E., (2003). A review of salt-fingering theory. This volume.

- Linden, P. F., (1974). Salt fingers in a steady shear flow. *Geophysical Fluid Dynamics*, 6, 1-27.
- McDougall T.J., & Taylor, J.R. (1984). Flux measurements across a finger interface at low value of stability ratio. *Journal of Marine Research*, 42, 1-14.
- Merryfield, W.J., & Grinder, M. Salt fingering fluxes from numerical simulations. unpublished.
- Moon, H.T., (1998). Flow of a vortex-pair street and the evolution of salt fingers. *Physical Review E*, 60(4), 4974-4977.
- Nagashima, H., Yoshida, J. & Nagahama, Y. (1997). A three dimensional modeling of salt-fingering convection. *Proc. Int. Congr. On Modeling and Simulation vol. 1* 189-191.
- Osborn, T.R., (1991). Observations of the salt fountain, *Atmosphere and Ocean*, 29(2), 340-356.
- Özgökmen, T.M., Esenkov, O.E. & Olson, D.B. (1998). A numerical study of layer formation due to fingers in double-diffusive convection in a vertically-bounded domain. *Journal Marine Research*, 56, 463-487.
- Özgökmen, T.M., & Esenkov, O.E. (1998). Asymmetric salt fingers induced by a nonlinear equation of state. *Physics of Fluids*, 10(8), 1882-1890.
- Piacsek, S.A., & Toomre, J. (1980). Nonlinear evolution and structure of salt fingers. In *Marine Turbulence*, ed. J.C.J. Nihoul, Elsevier Oceanography Series 28, 193-219.
- Piacsek, S.A., Brummell, N.H. & McDonald, B.E. (1988). Numerical experiments on thermohaline convective motions across interfaces of intrusions. In *Small Scale Turbulence and Mixing in the Ocean*, eds. J.C.J. Nihoul and B.M. Jamart, Elsevier

- Oceanography Series 46, 503-516.
- Radko, T., & Stern, M.E. (1999). Salt fingers in three dimensions. *Journal of Marine Research*, 57, 471-502.
- Radko, T., & Stern, M.E. (2000). Finite-amplitude salt fingers in a vertically bounded layer. *Journal of Fluid Mechanics*, 425, 133-160.
- Schmitt, R.W., (1979a). Flux measurements on salt fingers at an interface. *Journal Marine Research*, 37, 419-436.
- Schmitt, R.W., (1979b). The growth rate of super-critical salt fingers. *Deep-Sea Research*, 26A, 23-40.
- Schmitt, R.W., (1983). The characteristics of salt fingers in a variety of fluid systems, including stellar interiors, liquid metals, oceans, and magmas. *Physics of Fluids*, 26(9), 2373-2377.
- Schmitt, R.W., (1988). Mixing in a thermohaline staircase, In *Small Scale Turbulence and Mixing in the Ocean*, eds. J.C.J. Nihoul and B.M. Jamart, Elsevier Oceanography Ser., 46, 435-452.
- Schmitt, R.W., (1994). Triangular and asymmetric salt fingers. *Journal Physical Oceanography*, 24, 855-860.
- Schmitt, R.W., (1998). Double-diffusive convection: Its role in ocean mixing and parameterization schemes for large scale modeling. (Chapter in:) *Ocean Modeling and Parameterization*, eds. E. P. Chassignet and J. Verron, Kluwer Academic Publishers, 215-234.
- Schmitt, R.W., (2003). Observational and laboratory insights into salt-finger convection. This volume
- Shen, C.Y., (1989). The evolution of the double-diffusive instability: Salt fingers.

- Physics of Fluids*, A1(5), 829-844.
- Shen, C.Y. & Veronis, G. (1991). Scale transition of double-diffusive finger cells. *Physics of Fluids*, A3(1), 58-68.
- Shen, C.Y., (1993). Heat-salt finger fluxes across a density interface. *Physics of Fluids*, A5(11), 2633- 2643.
- Shen, C.Y., (1995). Equilibrium salt-fingering convection. *Physics of Fluids*, 7(4), 706-717.
- Shen, C.Y. & Veronis, G. (1997). Numerical simulation of two-dimensional salt fingers. *Journal of Geophysical Research*, 102(C10), 23131-23143.
- Shirtcliffe, T. G. L., & Turner, J.S. (1970). Observations of the cell structure of salt fingers. *Journal of Fluid Mechanics*, 41, 707-719.
- St. Laurent, L., & Schmitt, R.W. (1999). The contribution of salt fingers to vertical mixing in the North Atlantic Tracer Release Experiment. *Journal of Physical Oceanography*, 29, 1404-1424.
- Stern, M.E., (1960). The "salt-fountain" and thermohaline convection. *Tellus*, 12, 172-175.
- Stern, M.E., (1969). Collective instability of salt fingers. *Journal of Fluid Mechanics*, 35(2), 209-218.
- Stern M.E., & Radko, T. 1998. The salt finger amplitude in unbounded T-S gradient layers. *Journal Marine Research*, 56, 157-196.
- Stommel, H., Arons, A.B., & Blanchard, D. 1956. An oceanographic curiosity: the perpetual salt fountain. *Deep-Sea Research*, 3,152-153.
- Taylor J.R., & Bucens, P. (1989). Laboratory experiments on the structure of salt fingers. *Deep-Sea Research*, 36(11), 1675-1704.

- Taylor, J., & Veronis, G. (1996). Experiments on double-diffusive sugar-salt fingers at high stability ratio. *Journal of Fluid Mechanics*, 321, 315-333.
- Turner, J.S., & Stommel, H. (1964). A new case of convection in the presence of combined vertical salinity and temperature gradients. *Proceeding of National Academy of Science. U.S.A.*, 52, 49-53.
- Turner, J.S., (1967). Salt fingers across a density interface. *Deep-Sea Research*, 14, 599-611.
- Veronis, G., (1987). The role of the buoyancy layer in determining the structure of salt fingers. *Journal of Fluid Mechanics*, 180, 327-342.
- Whitfield, D.W.A., Holloway, G., & Holyer, J.Y. (1989). Spectral transform simulations of finite amplitude double-diffusive instabilities in two dimensions. *Journal Marine Research*, 47(2), 241-265.

## Figure Captions

Figure 1 Evolution of salt-fingers together with temperature and salt profiles. Salinity field is presented on the left. In this case,  $R\rho$  is taken to be 3. (Piacsek and Toomre (1980))

Figure 2 Evolution of salt-fingers from Whitfield et al. (1989). Salinity field is presented. In this case,  $R\rho$  is taken to be 1.33,  $\sigma = 3$ ,  $\tau = 1/3$ .

Figure 3 Evolution of salt-fingers. Temperature and salinity fields are presented. In this case,  $\sigma = 1$ ,  $\tau = 1/10$ , and  $R\rho$  is taken to be 2. (Reprinted with permission from Shen, C.Y., 1989, The evolution of the double-diffusive instability: Salt-fingers. *Physics of Fluids*, A1(5), 829-844. copyright 1989, American Institute of Physics).

Figure 4 Evolution of domain-averaged density(left), temperature(right, solid lines) and salinity(right, dashed lines) profiles. (Reprinted with permission from Shen, C.Y., 1989, The evolution of the double-diffusive instability: Salt-fingers. *Physics of Fluids*, A1(5), 829-844. copyright 1989, American Institute of Physics).

Figure 5 Flux ratio  $Rf$ ,  $C$  and Stern number  $A$  as functioned  $R\rho$ . Solid diamonds are from the numerical experiment. Other symbols are from laboratory experiments (Schmitt, 1979a; Taylor & Bucens, 1989; Turner, 1967; McDougall and Taylor, 1984). (Reprinted with permission from Shen, C.Y., 1993. Heat-salt finger fluxes across a density interface. *Physics of Fluids*, A5(11), 2633- 2643. copyright 1993, American Institute of Physics).

Figure 6 Contour plots of temperature (upper left), salinity (upper right), density (lower right) and stream function(lower right). Domain size is 22cm  $\times$  44cm.(Shen and Veronis, 1997).(Reproduced by permission of American Geophysical Union)

Figure 7 Stream-function  $\Psi$  (Top left of each three pair of contour lines), temperature  $T$  (top middle) and salinity  $S$  (top right) fields, and vertical profiles of temperature  $T$  (lower left), salinity  $S$  (lower middle) and density  $\rho$  (lower right) for (a)  $t=0.3$ , (b)  $t=0.5$  and (c)  $t=1.7$  (Özgökmen et al., 1998).

Figure 8 Instantaneous salinity field for equilibrated salt fingers for  $R\rho=1.25, 1.5, 4$  and 15. (Merryfield & Grinder, unpublished).

Figure 9 Comparison of vertical diffusivities of salt ( $K_S$ ) and heat ( $K_T$ ) obtained by numerical simulation (solid curves, Merryfield & Grinder, unpublished) and observations ( ; NATRE site, St. Laurent and Schmitt, 1999; C-SALT, Fleury & Lueck, 1991).

Figure 10 Comparison between horizontal temperature gradient spectra for  $R\rho=1.5$  (heavy solid line) and  $R\rho=2.0$  (thin solid line) from the numerical calculations of Merryfield & Grinder (unpublished) and that obtained by Fleury & Lueck (1991) for  $R\rho=1.6$  (dashed line). ( ).

Figure 11 Density flux ratio  $\gamma$  is plotted against  $R\rho$  (solid circles with error bars) together with theoretically obtained flux ratio for the fastest growing salt finger (continuous curve, Schmitt, 1979a). Also shown by open circles are estimated from Shen (1995). (Merryfield & Grinder, unpublished).

Figure 12 Development of fingers (left) and magnified view of the mushroom structure (right). (Nagashima et al., 1997). (Reproduced by permission of Modelling and Simulation Society of Australia and New Zealand).

Figure 13 Plan view of salt fingers at middepth. The salinity difference  $\Delta S$  of Case 3 (right) is 16 times greater than that in Case-1 (left). (Nagashima et al., 1997). ). (Reproduced by permission of Modelling and Simulation Society of Australia and New Zealand)

Figure 14 Horizontal temperature cross section obtained by Radko and Stern (1999). Solid and dashed lines correspond to high (down-going finger) and low (up-going finger) temperature area, respectively.

Figure 15 Vertical temperature cross section by Radko and Stern (1999). Solid and dashed lines are the same as in Figure 14.

Figure 16 Horizontal cross-section of temperature at a) mid-depth and b) near the boundary. Vertical cross section of temperature is also shown on the right (Radko and Stern, 2000). (Reprinted with the permission from Cambridge University Press).

Figure 17 Time sequences of transition from rolls to square cell. Left panels; Horizontal cross sections of temperature field at mid-depth. Right panel; Same as on the left but near the upper boundary (Radko and Stern, 2000). Times shown are (a)  $t=0$ , (b)  $t=400$  and (c)  $t= 4600$ . (Reprinted with the permission from Cambridge University Press).

Figure 18 Vertical temperature cross section in the boundary layer near  $z=H$  for relatively (a) small and (b) large Rayleigh number (Radko and Stern, 2000). (Reprinted with the permission from Cambridge University Press).

Figure 19 Proportionality constants  $C$  of the 4/3 flux law, plotted against density ratio. (a) Asymptotic analysis (solid curve) is compared with the results of numerical calculations (symbols). (b) Experimental results by Taylor and Veronis (1996) (symbols) are compared with asymptotic analysis (solid curve, same as in Figure 19a). Other laboratory results are averaged and is shown by the straight line (Radko and Stern, 2000). (Reprinted with the permission from Cambridge University Press).

Table 1 Governing parameters

Parameters	definitions
Prandtl number	$\sigma = \frac{\nu}{\kappa_T}$
Thermal Rayleigh number	$R_T = \frac{g \alpha \Delta T d^3}{\kappa_T \nu}$
Saline Rayleigh number	$R_S = \frac{g \beta \Delta S d^3}{\kappa_T \nu}$
Lewis number	$\tau = \frac{\kappa_S}{\kappa_T}$
Schmidt number	$Sc = \frac{\nu}{\kappa_S}$
Density anomaly ratio	$R\rho = \frac{\alpha \Delta T}{\beta \Delta S}$
Stern number	$St = \frac{g\beta F_S - g\alpha F_T}{\nu N^2}$

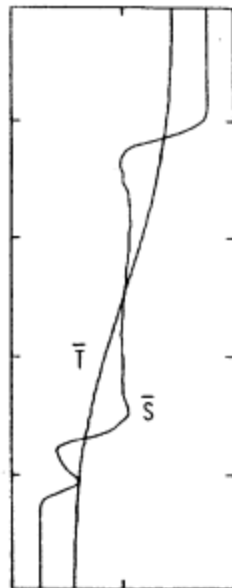
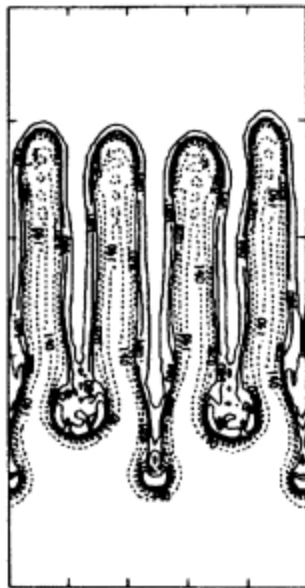
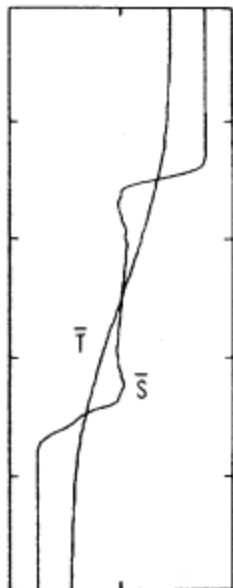
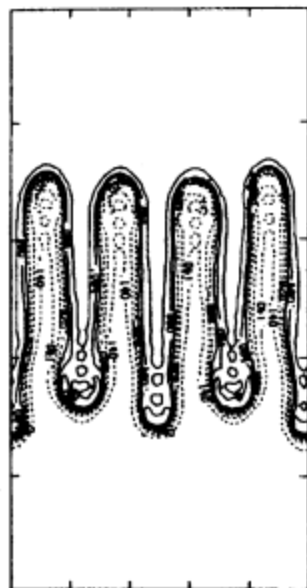
Table 2 Governing parameters for selected two-dimensional experiments. Note that

$\sigma = 7$  and  $\tau = 1/100$  cases are heat/salt-finger experiments.

	$\sigma = \frac{\nu}{\kappa_T}$	$\tau = \frac{\kappa_S}{\kappa_T}$	$R\rho = \frac{\alpha \Delta T}{\beta \Delta S}$	$R_T = \frac{g \alpha \Delta T d^3}{\kappa_T \nu}$	$N$
Piacsek and Toomre(1980)	6.8	1/100	3.5, 7	$10^6$	2-layers
Whitfield et al. (1989)	3, 10	1/10,1/3 ,1/2	1.1-2.5 (6 cases)	Not specified  $6.2 \times 10^2$	Linear
Shen (1989)	1, 2	1/10,1/2	2	$4.9 \times 10^2$  $1.5 \times 10^2$	2-layers
Shen (1993)	7	1/100	1.2,1.5,2.0 2.5,3.0,4.0	$(1.2 - 4.0) \times 10^7$	2-layers
Shen (1995)	7	1/100	2.0,3.0,4.0, 8.0	$1.33 \times 10^7$	Linear
Shen and Veronis (1997)	7	1/80	15, 3.0	$1.54 \times 10^3 -$ $2.74 \times 10^6$ (5 cases)	2-layers
Özgökmen et al. (1998)	100	1/30	1.6	$6 \times 10^7$	Linear
Merryfield and Grinder (unpublished)	7	1/100	1.25-20 (13 cases)	$6 \times 10^6$ (for $R\rho = 2$ )	Linear

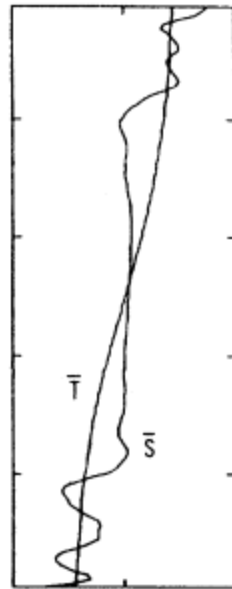
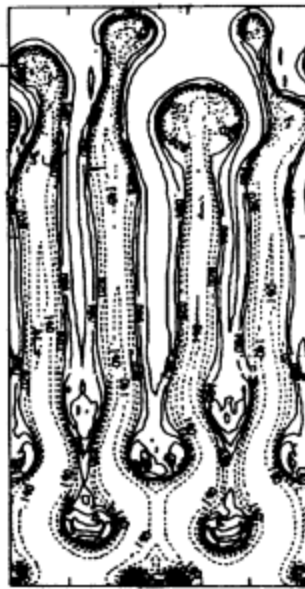
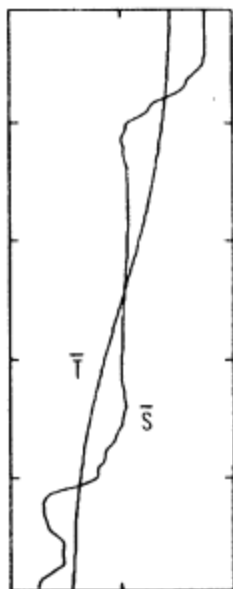
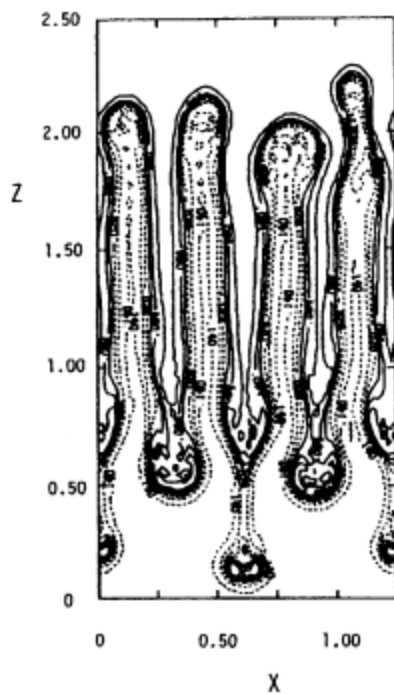
60 SEC

70 SEC



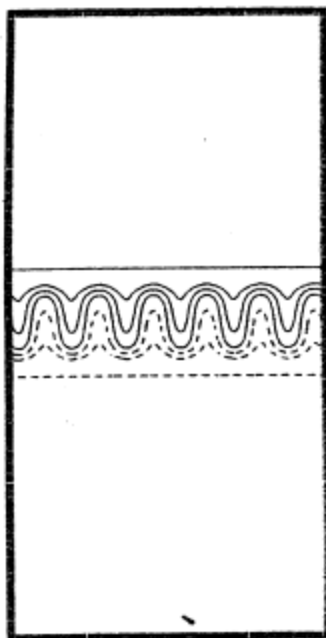
80 SEC

90 SEC

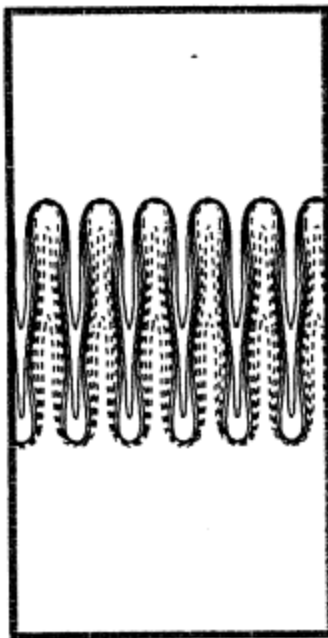

 $\Delta = 3$  1.25 x 2.50 cm

# Figure 1

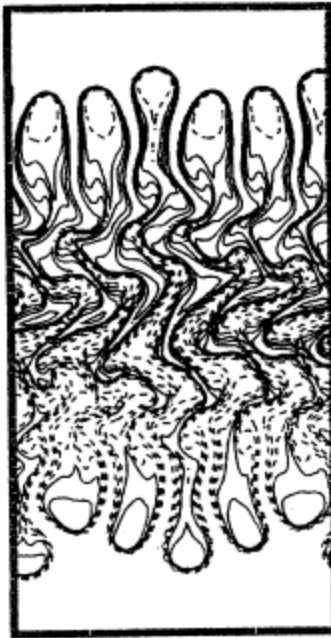
SALINITY



t=10



t=15



t=19



t=20

Figure 2

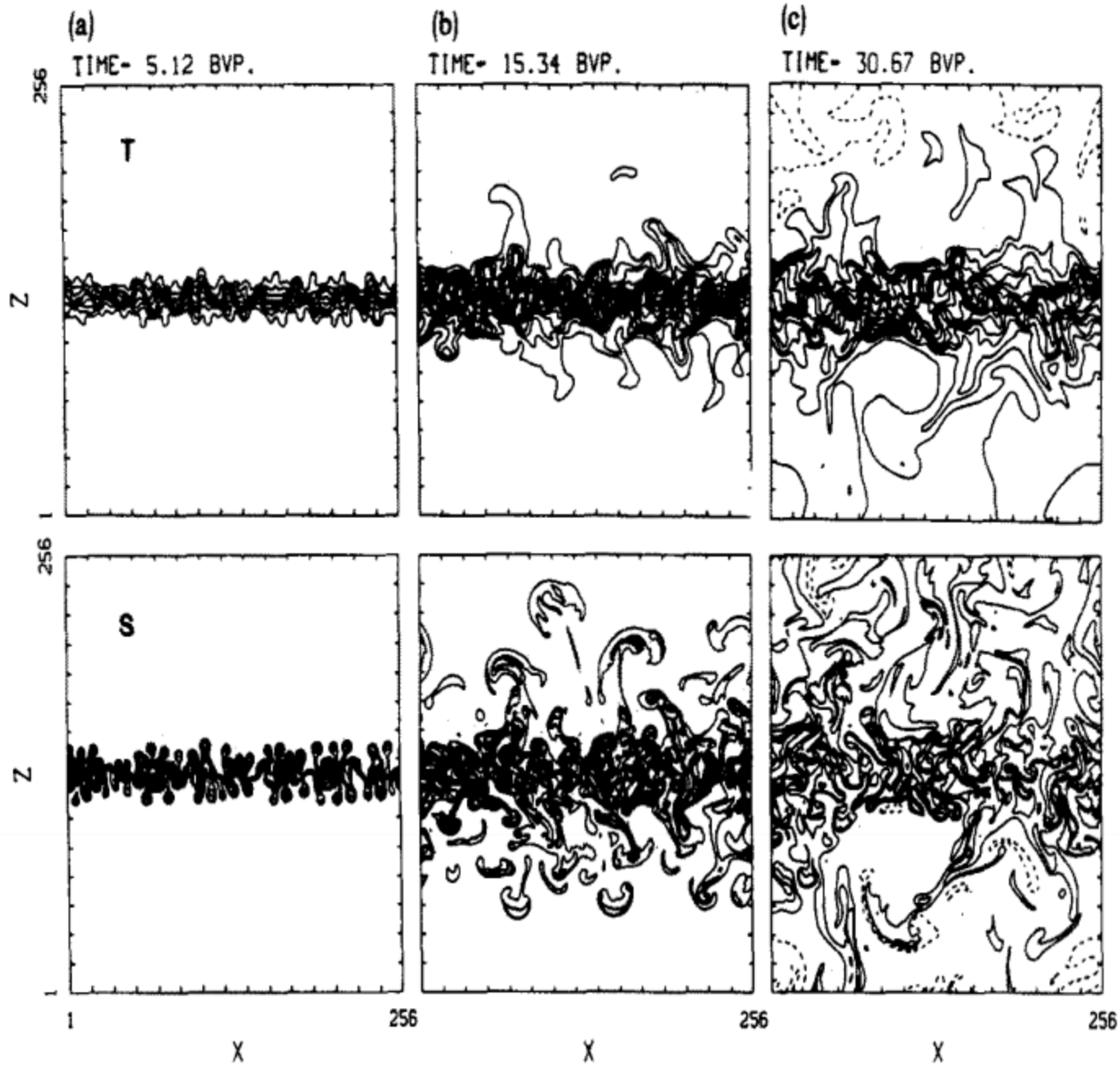


Figure 3

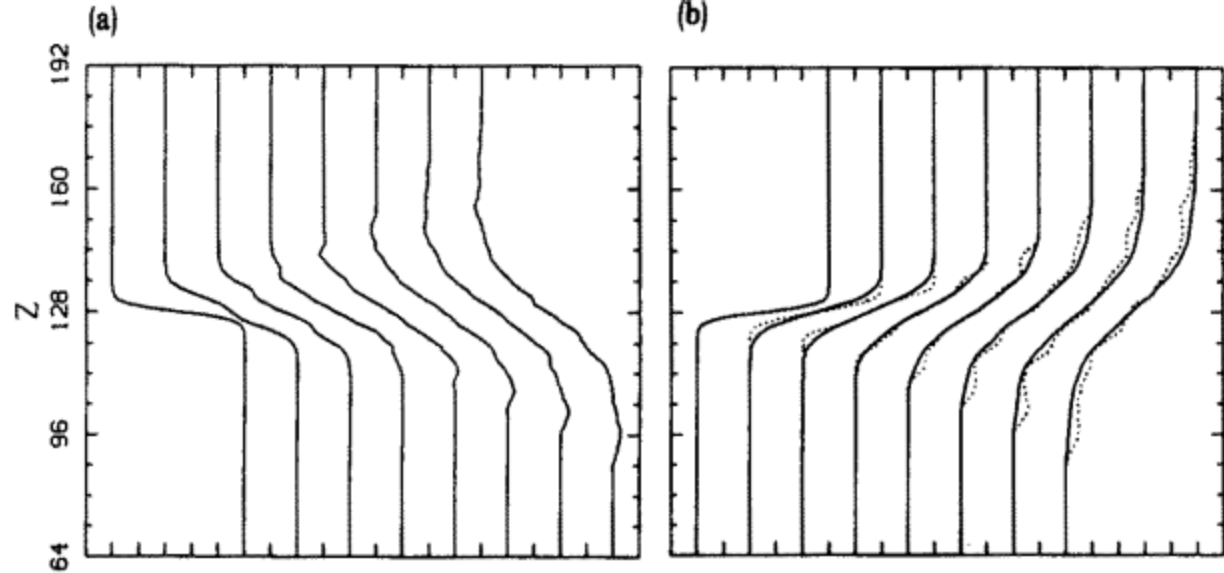


Figure 4

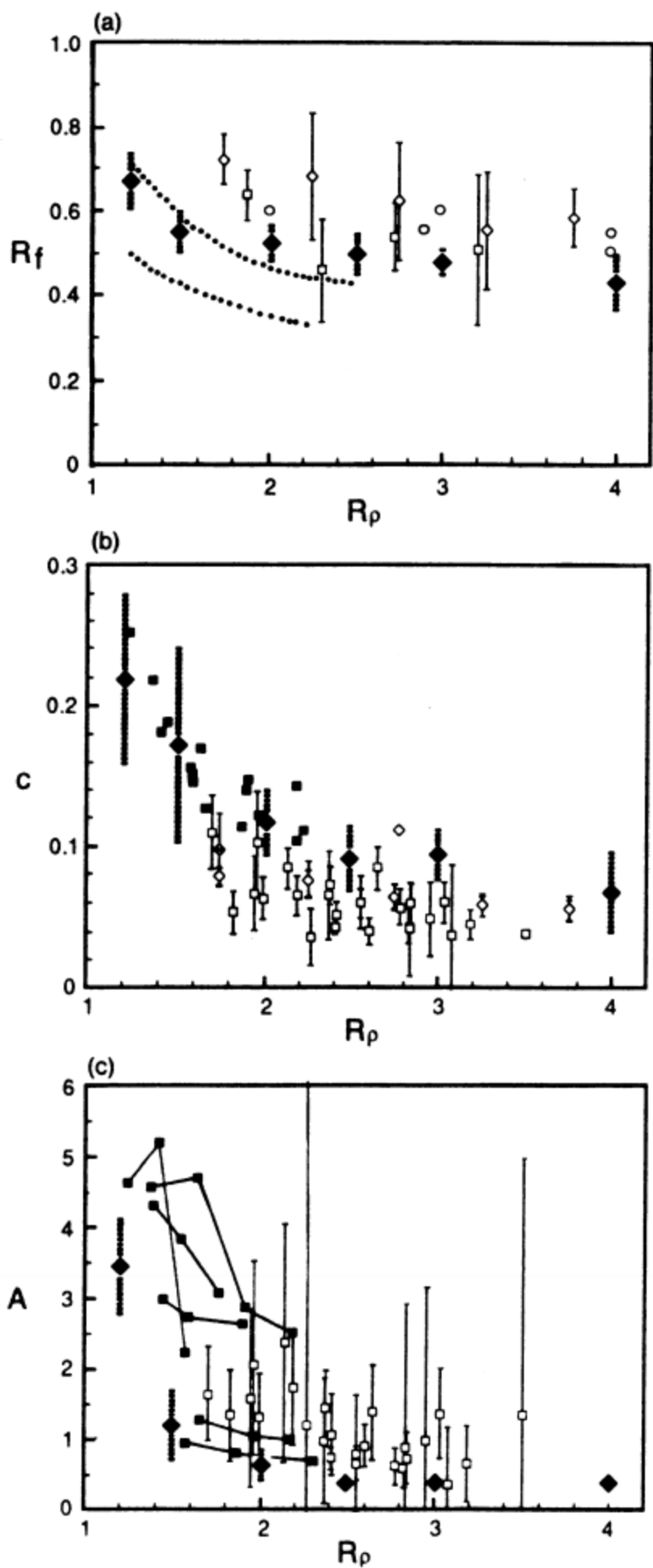


Figure 5

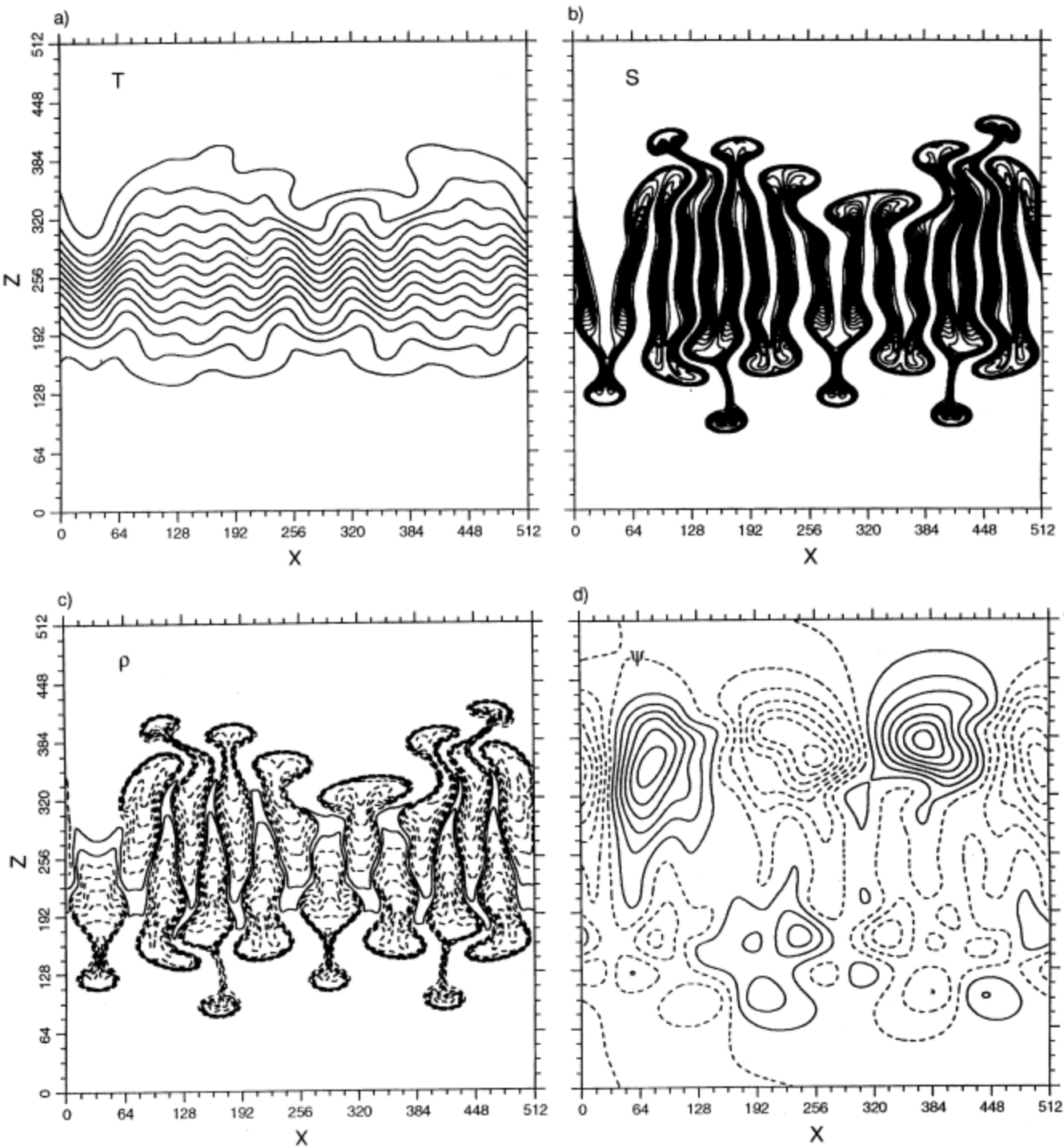


Figure 6

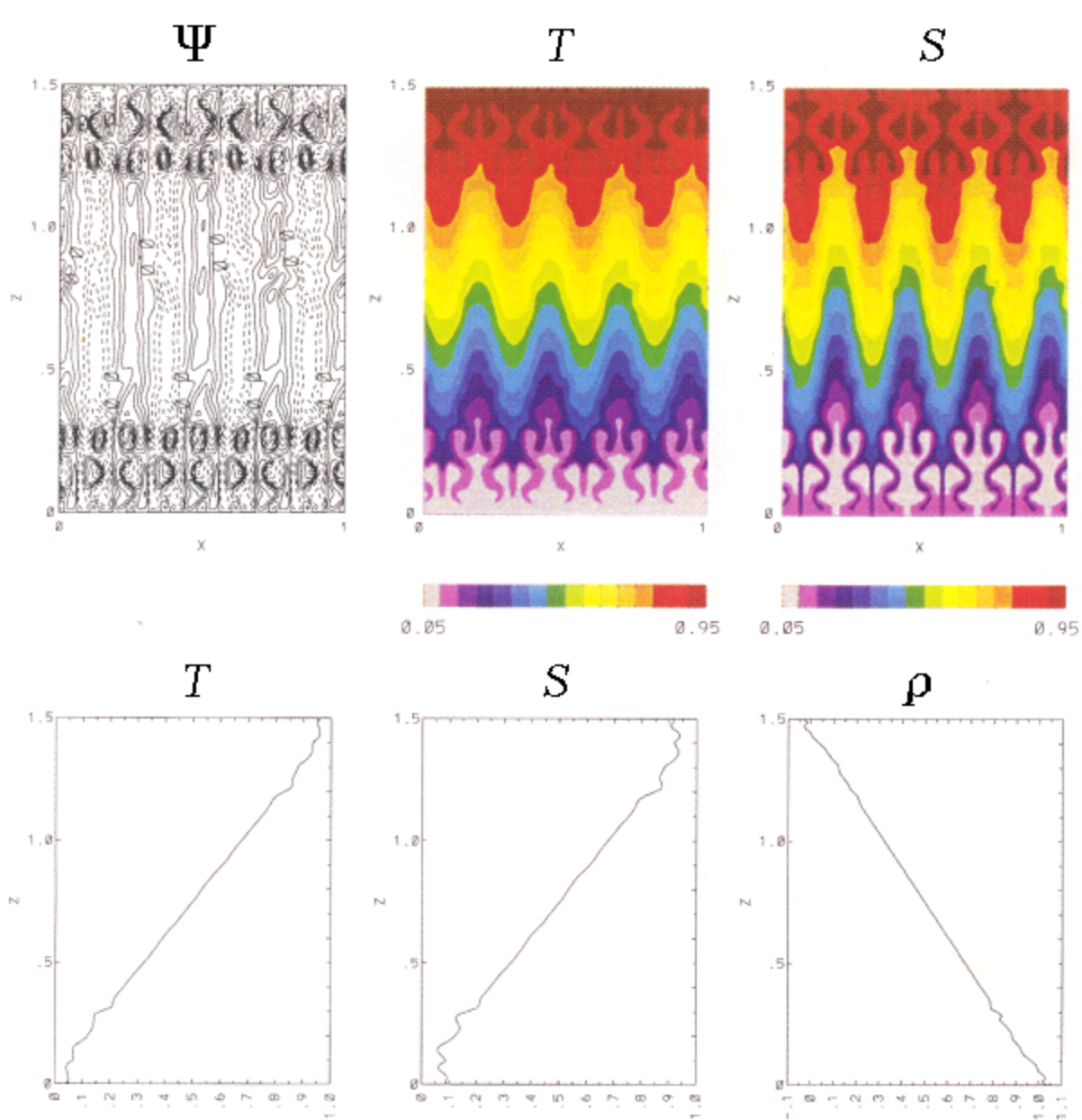
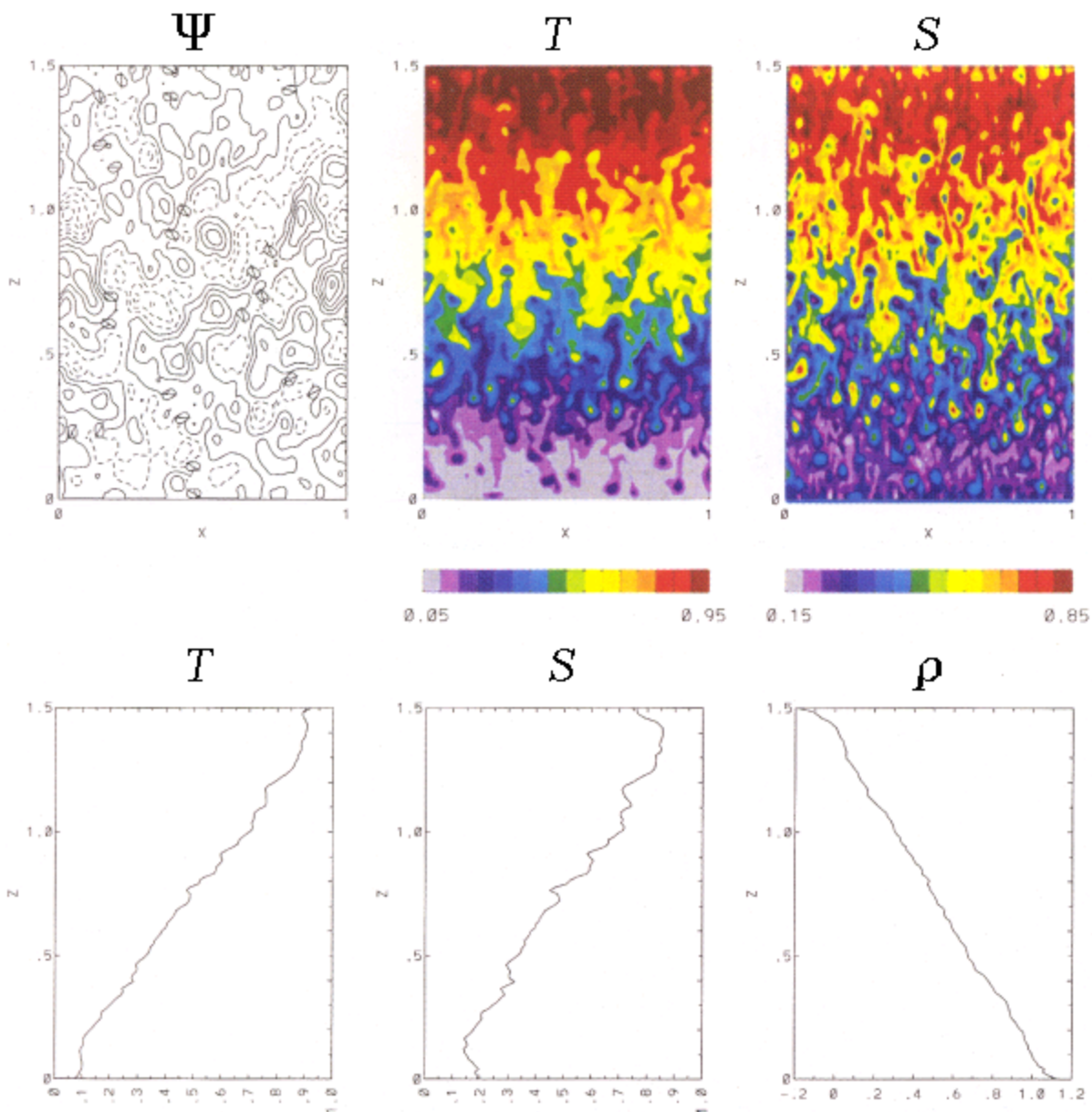


Figure 7(a)



**Figure 7(b)**

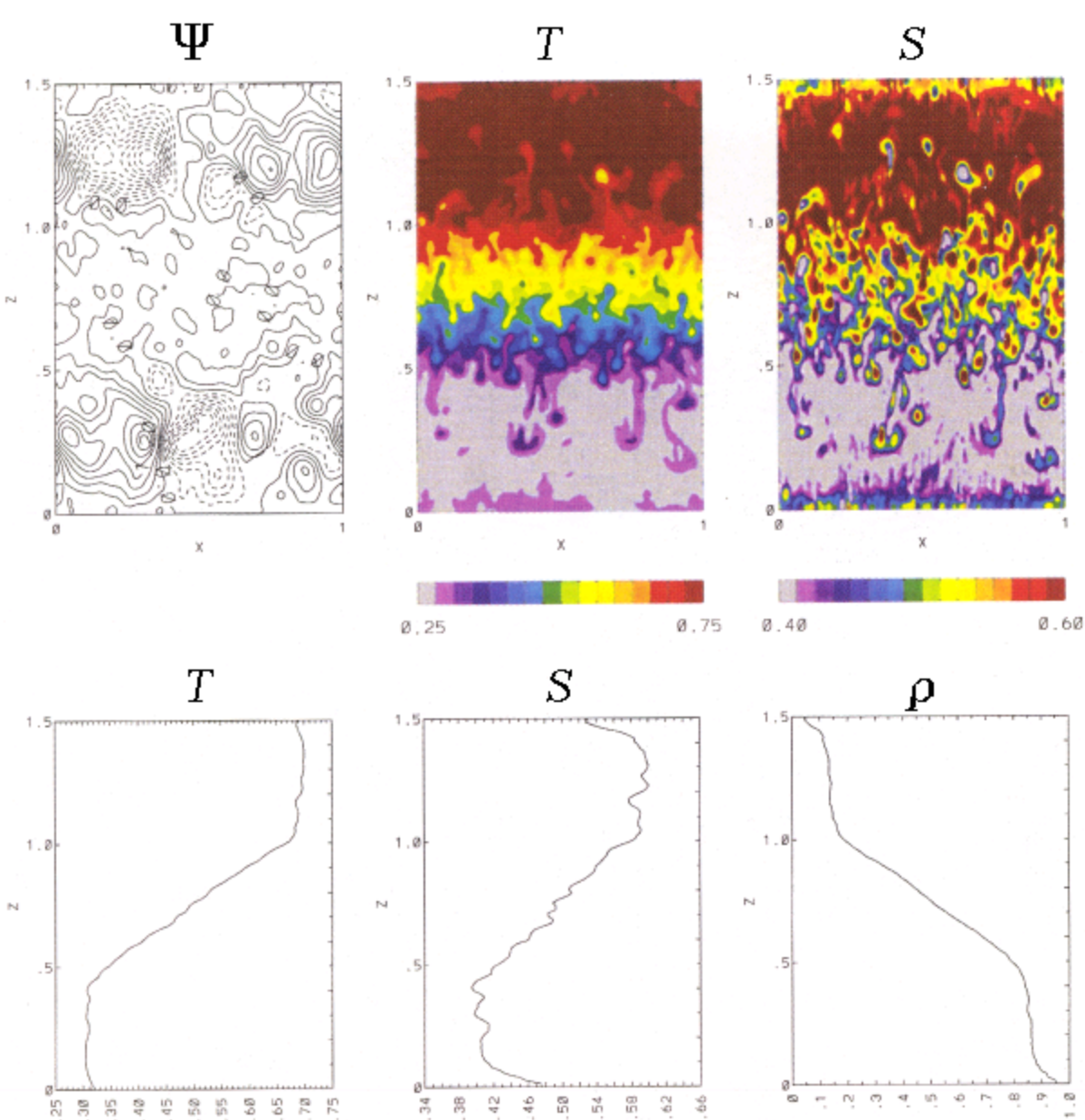
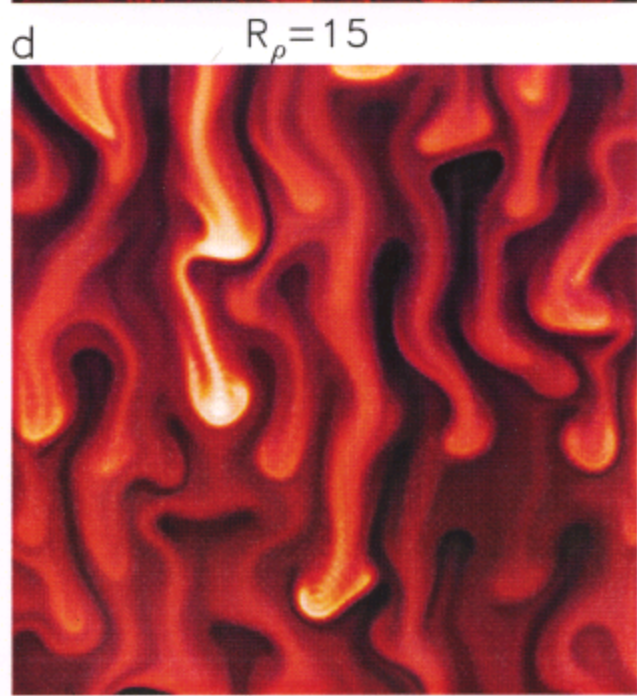
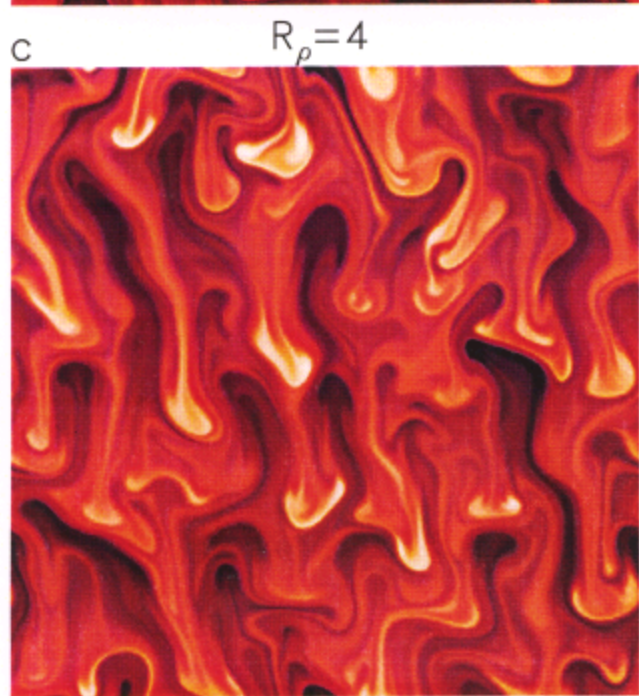
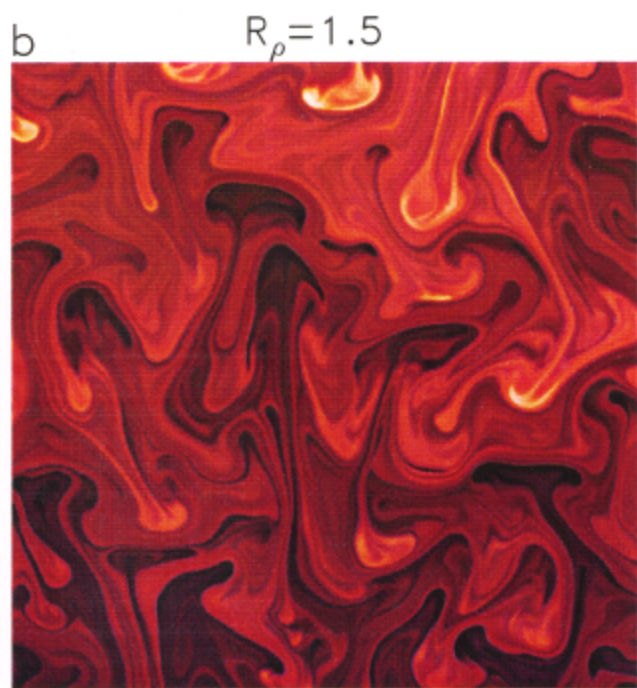
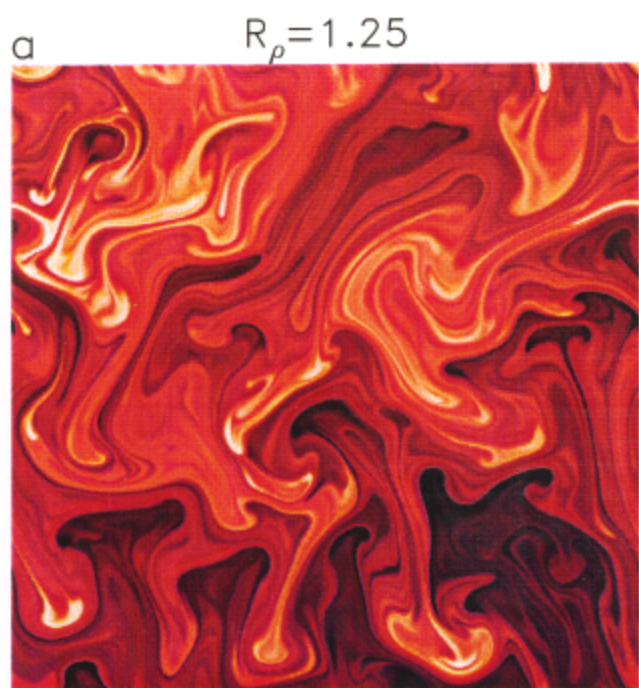


Figure 7(c)



**Figure 8**

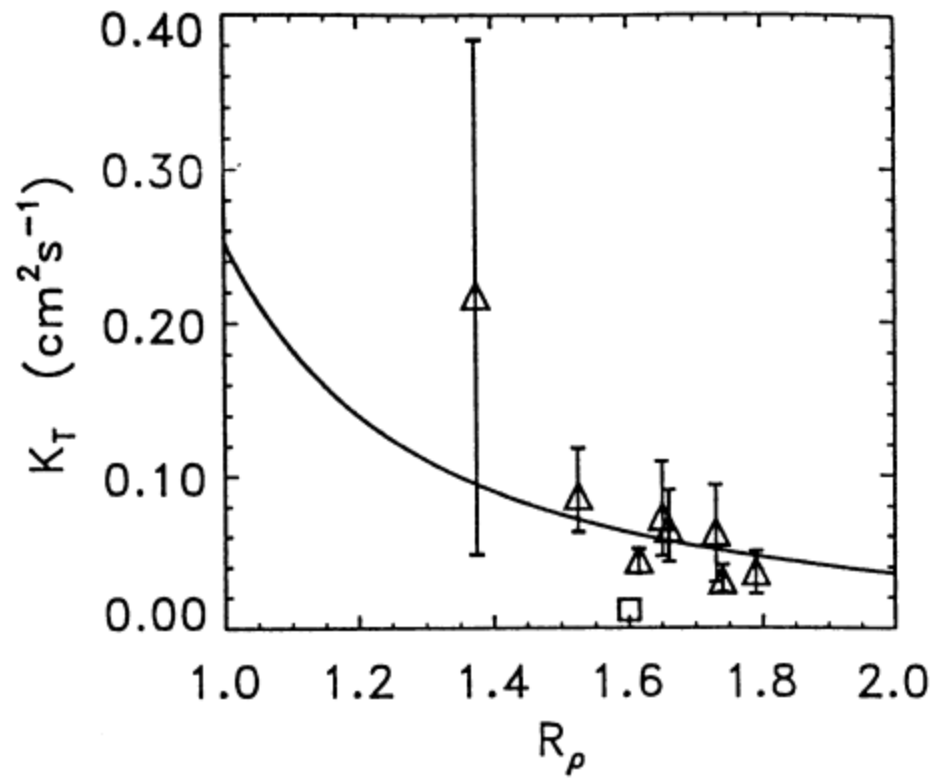
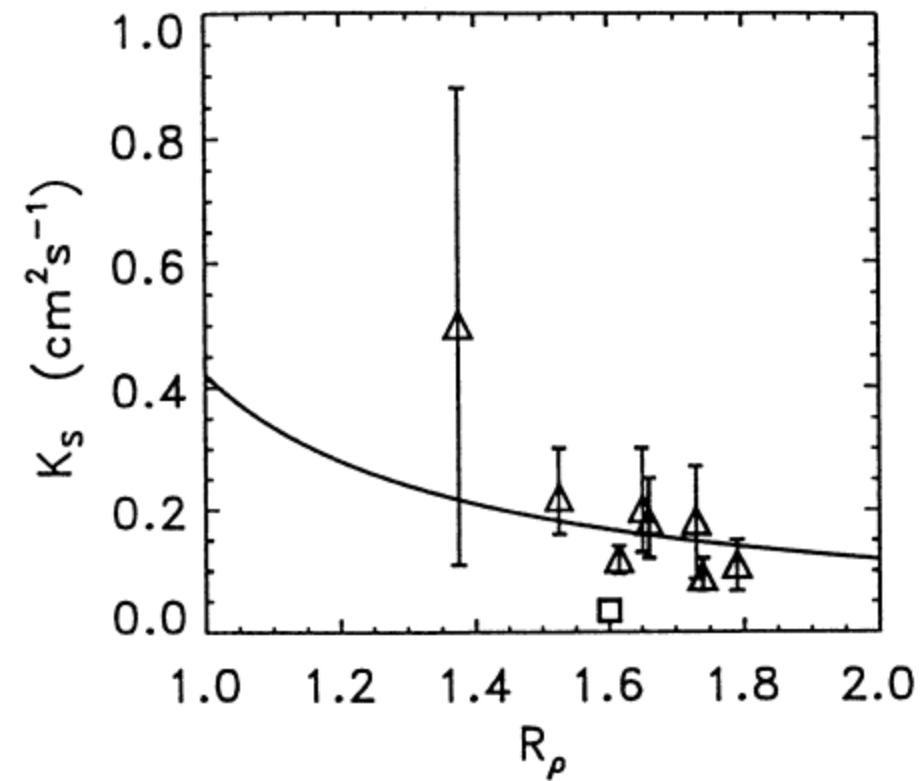
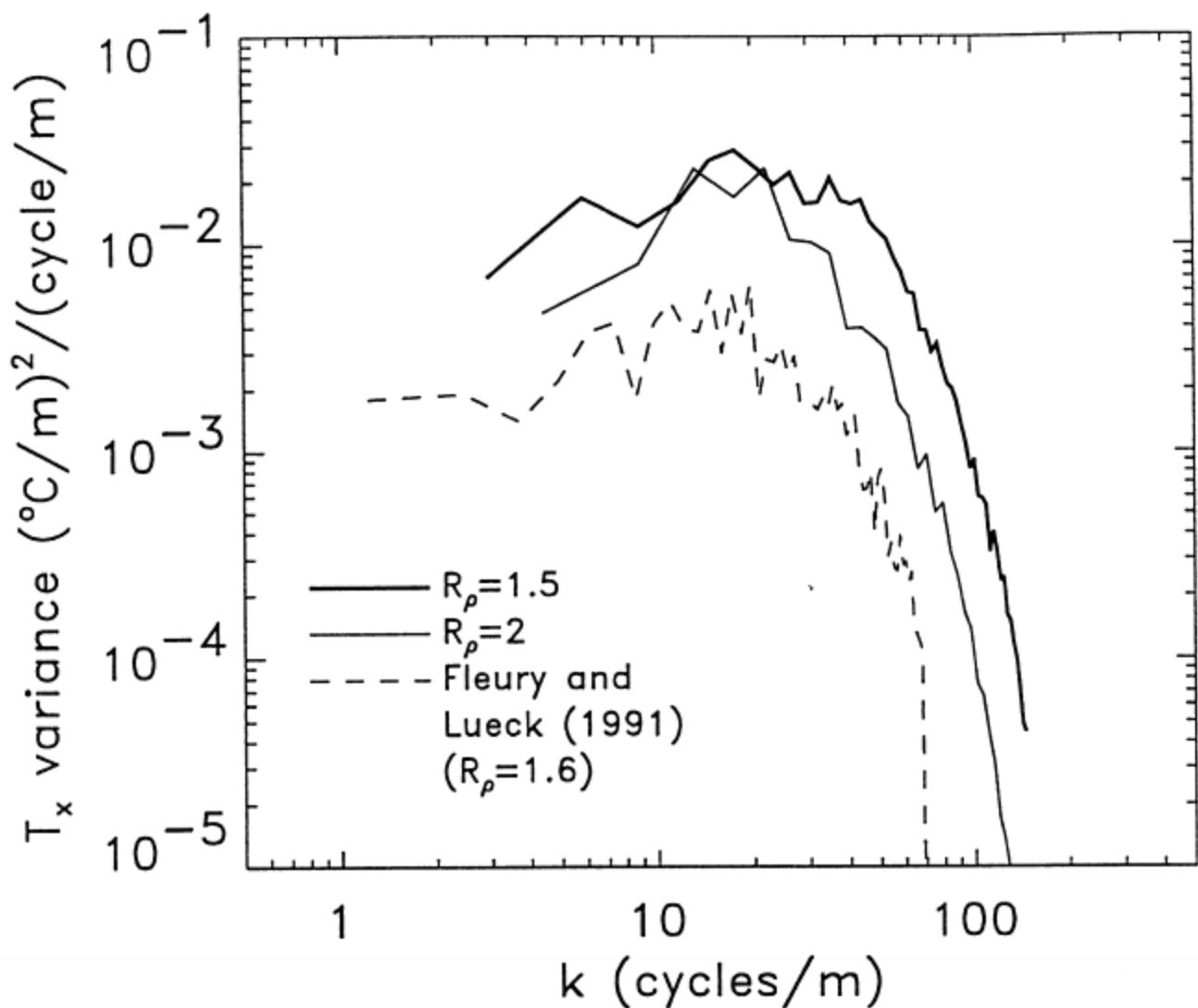
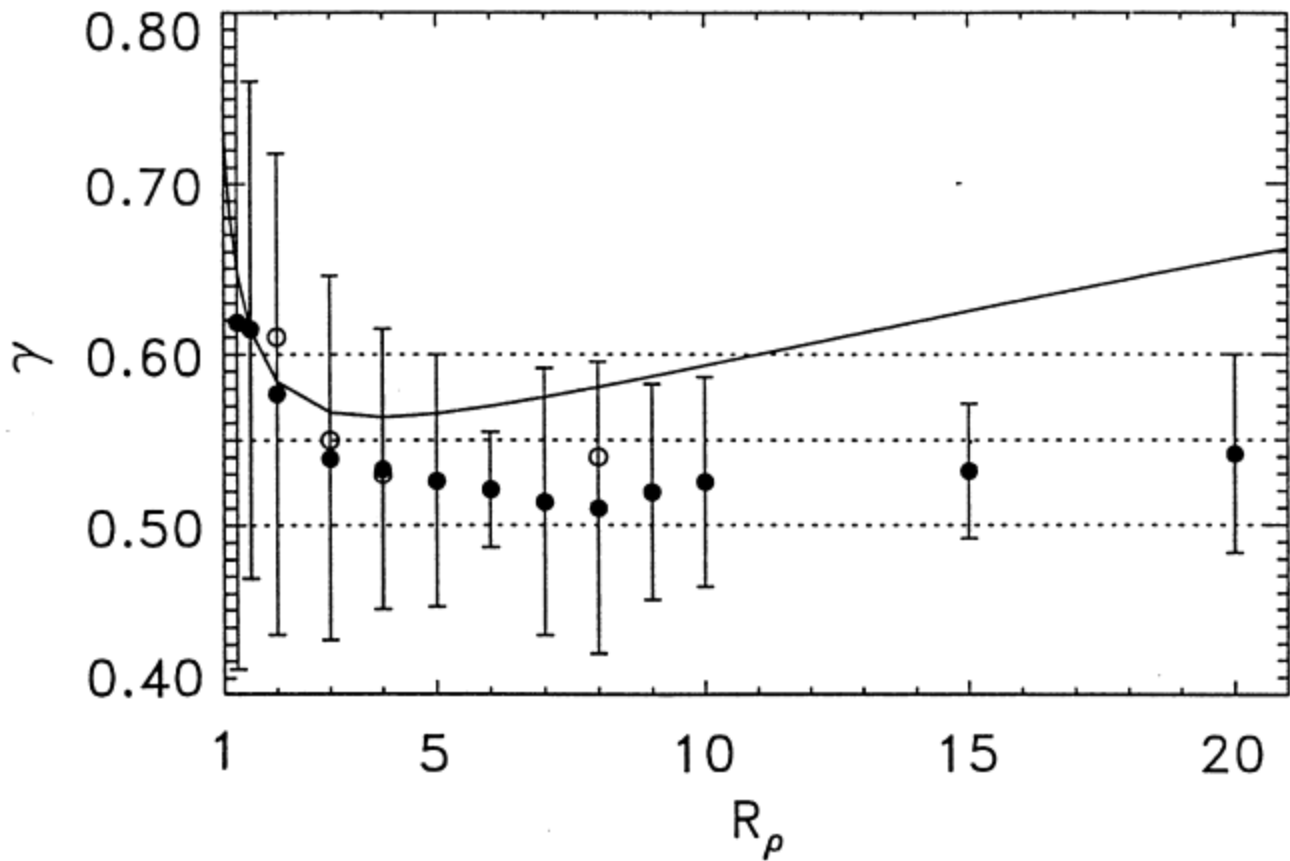


Figure 9



**Figure 10**



**Figure 11**

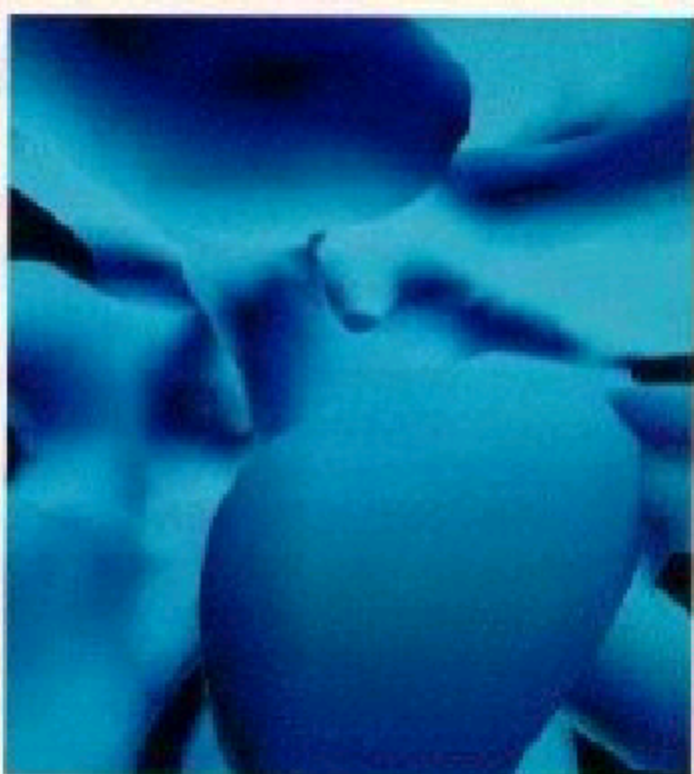
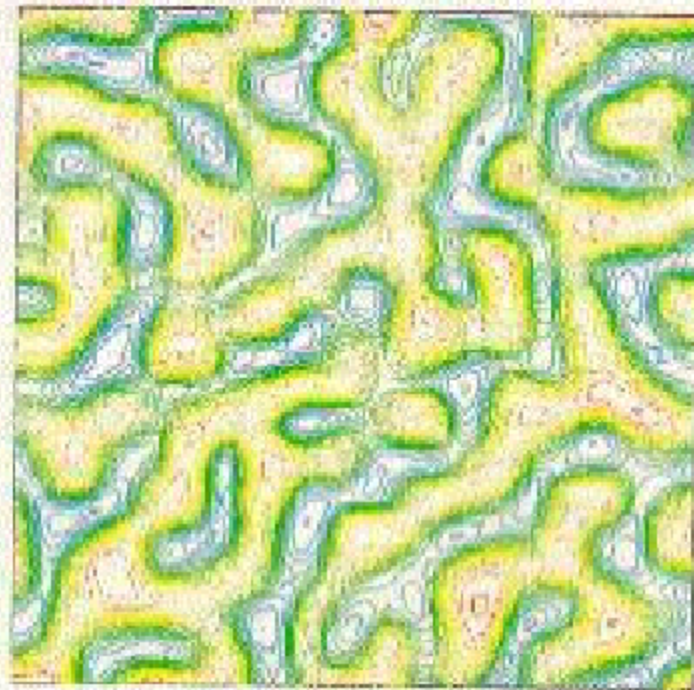
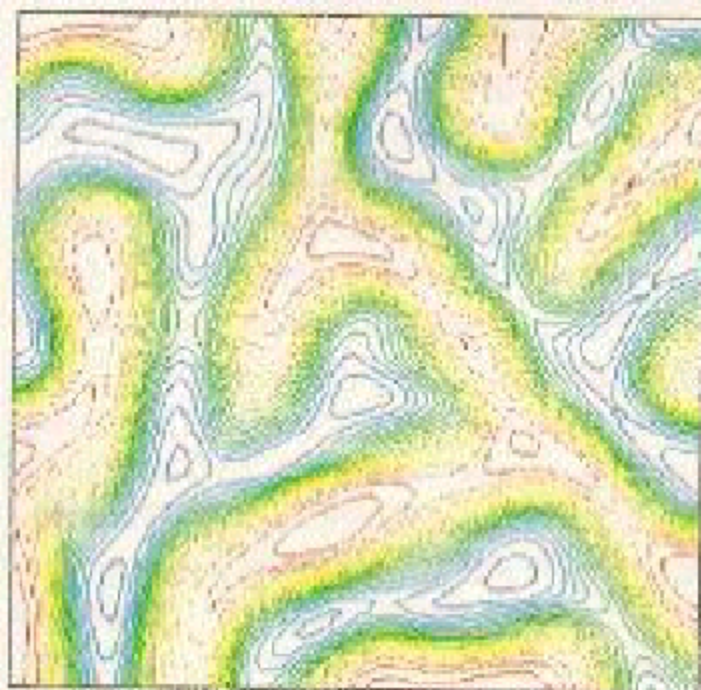


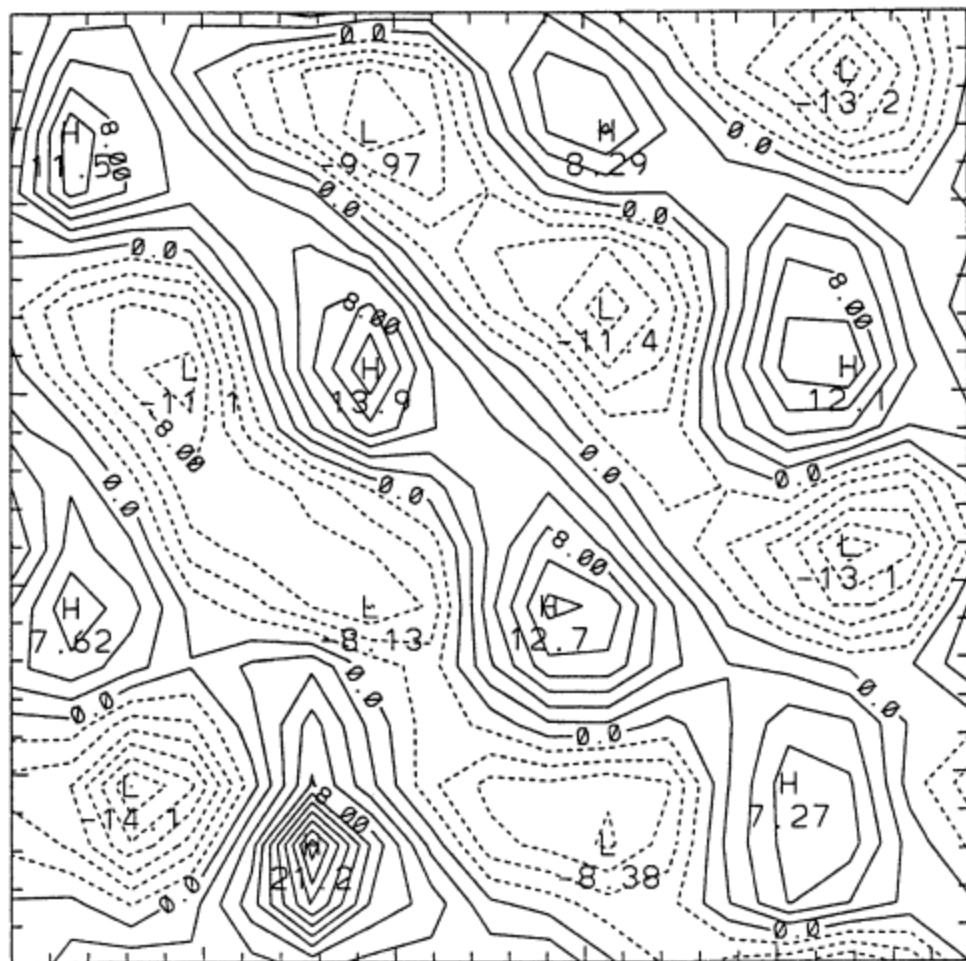
Figure 12



**Figure 13**

$T(x,y,0)$

$y=45.1$



$y=0$

$x=0$

$x=45.1$

**Figure 14**

$T(x,0,z)$

$$z = \frac{2\pi}{m} = 160.$$

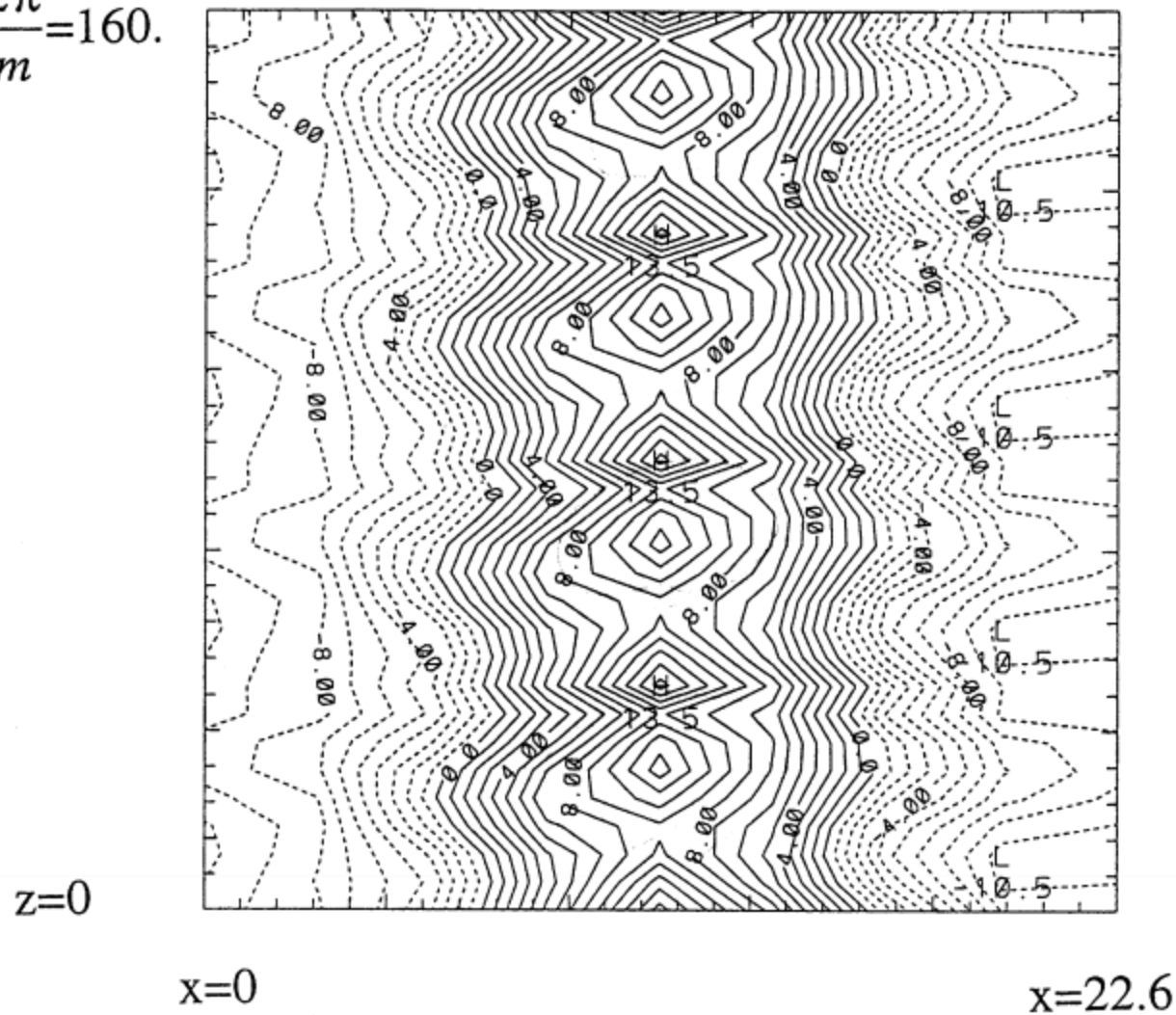


**Figure 15**

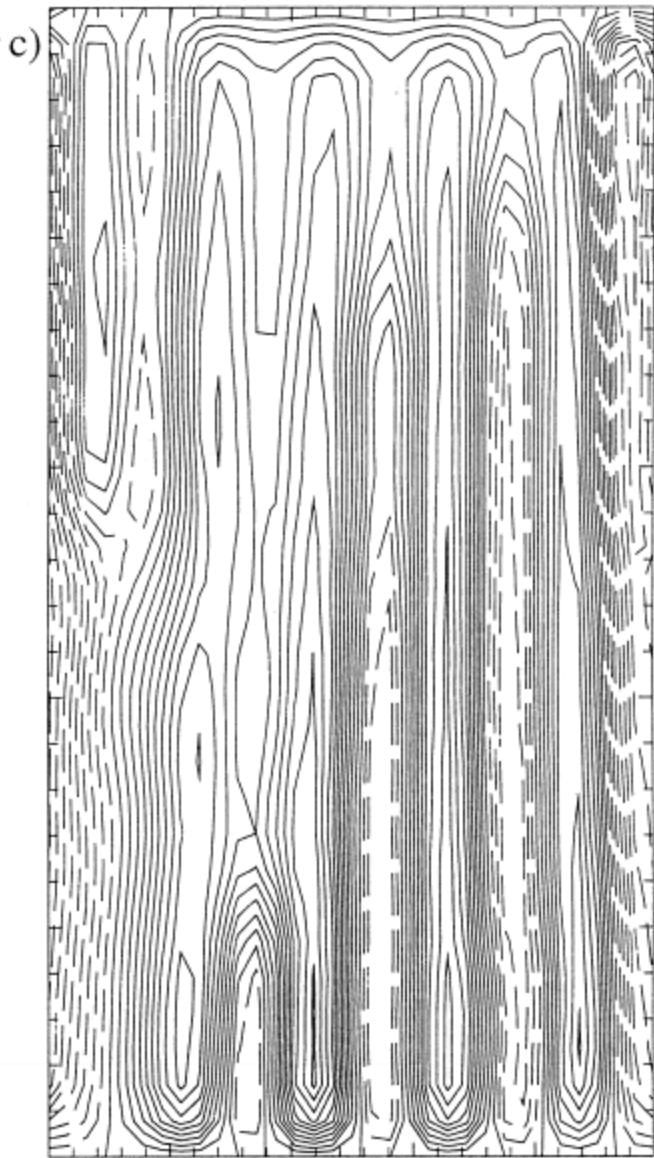
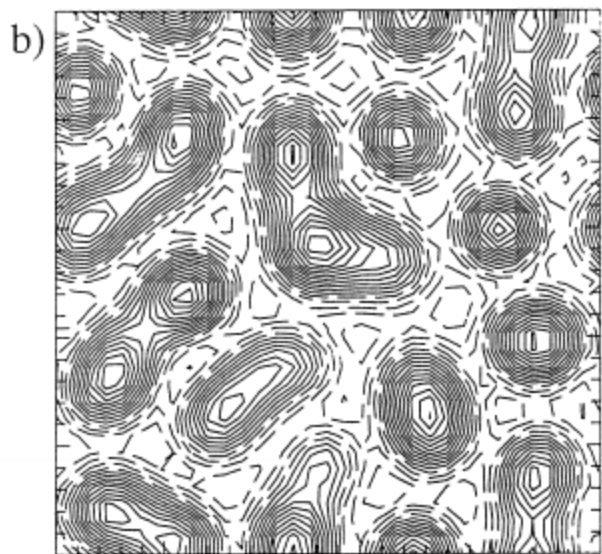
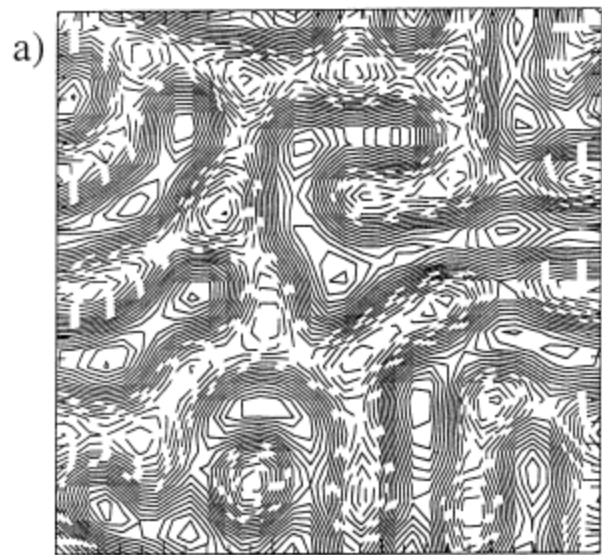
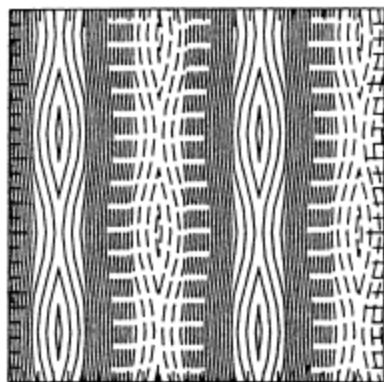


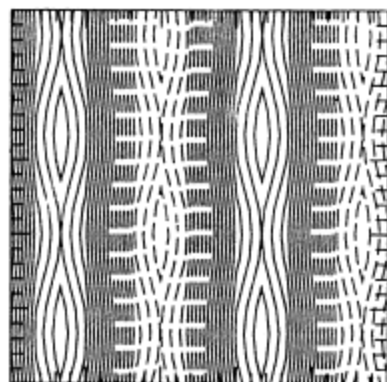
**Figure 16**

$$z = \frac{H}{2}$$

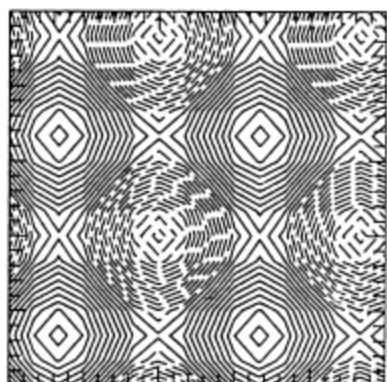
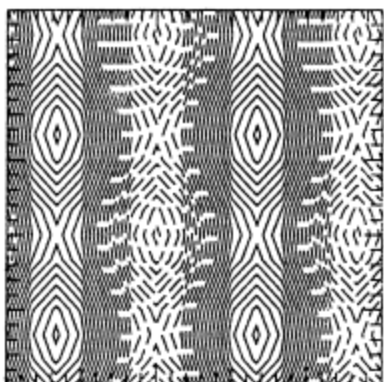
a)



$$z = \frac{H}{64}$$



b)



c)

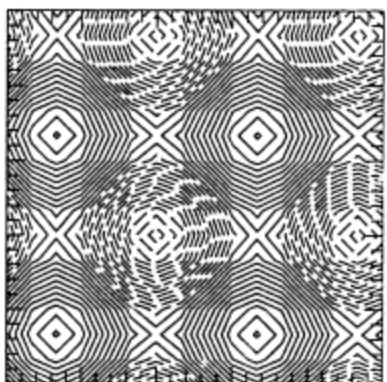
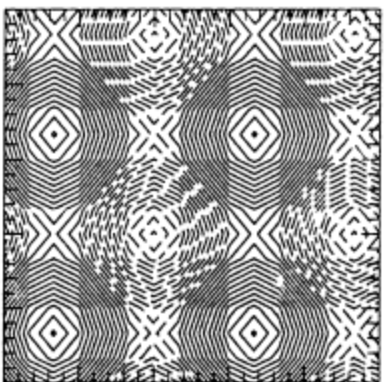
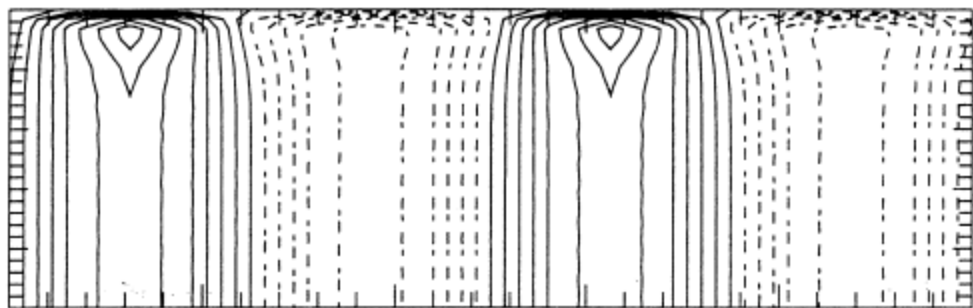


**Figure 17**

$\mu=1:50, Ra=1440, R=1.6$

a)



$\mu=1:100, Ra=2800, R=1.6$

b)

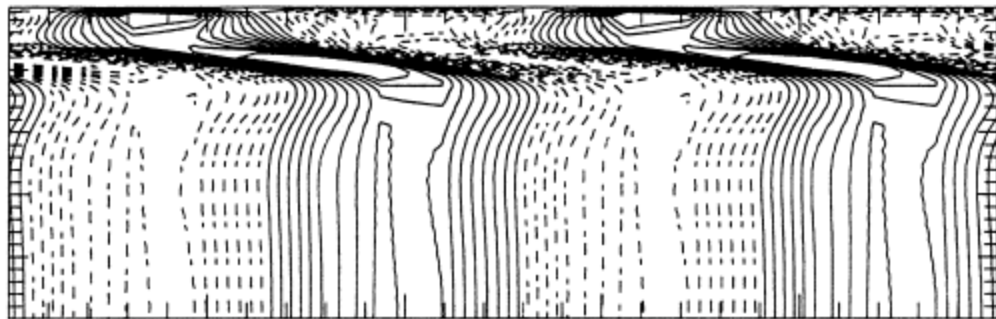


**Figure 18**

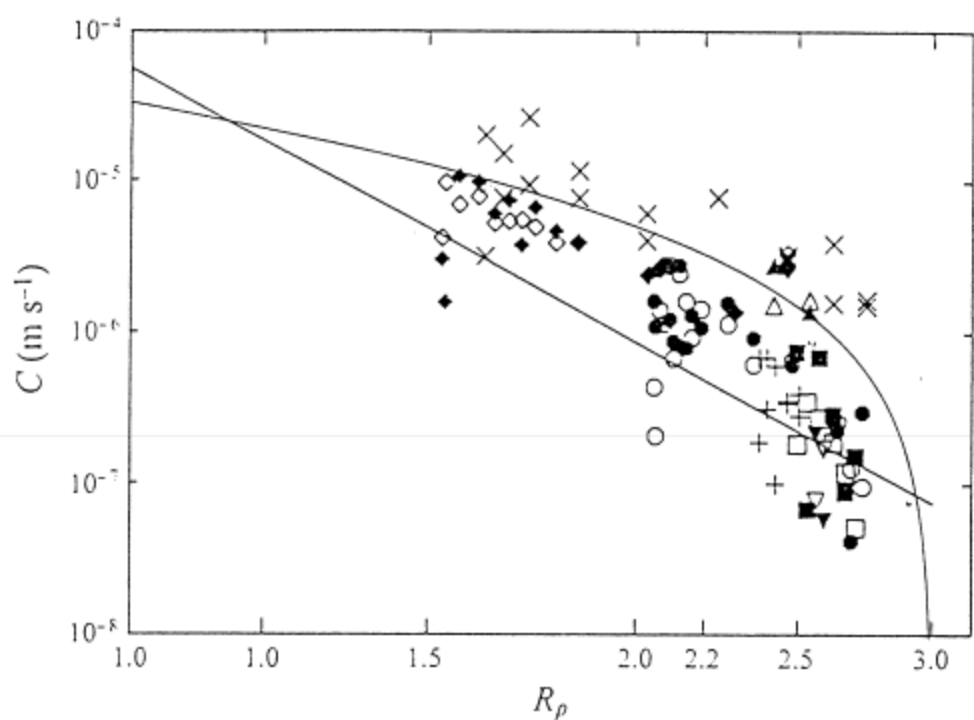
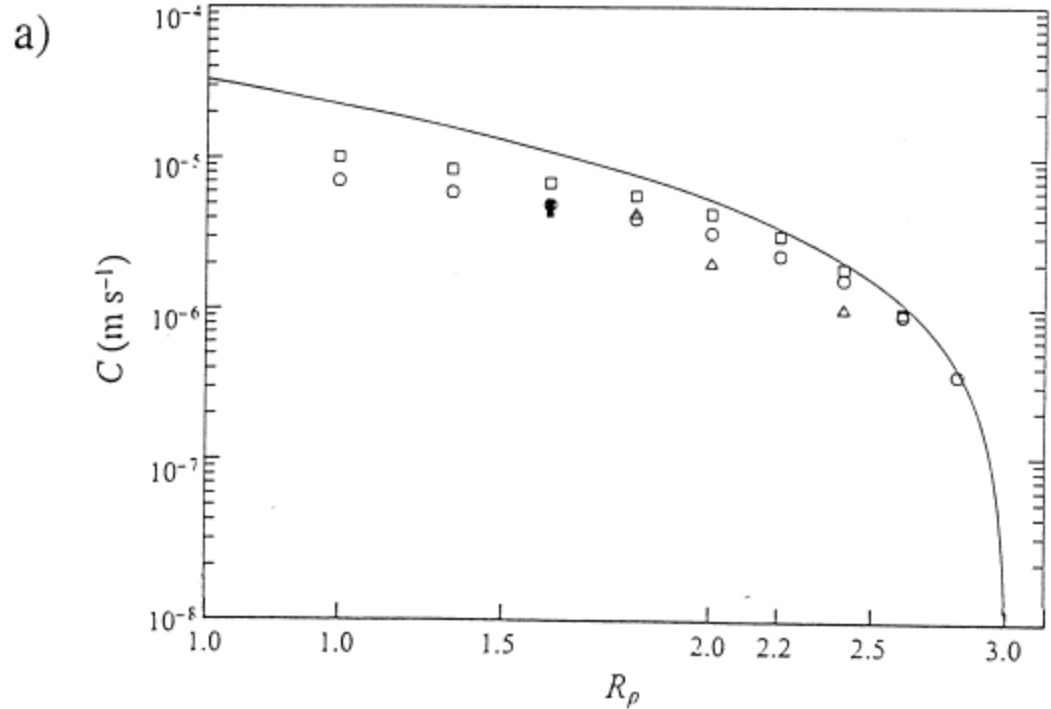


**Figure 19**